CENTRO DE INVESTIGACIÓN Y DE ESTUDIOS AVANZADOS
DEL INSTITUTO POLITÉCNICO NACIONAL
UNIDAD MONTERREY

Modelo Matemático Para la Liberación de Calcio a Través de Receptores de Rianodina y la Dinámica Calcio-Calsecuestrina en Células de Músculo Liso

Tesis que presenta

Laura Sánchez Gómez

para obtener el grado de

Maestra en Ciencias

con especialidad en

Ingeniería y Física Biomédicas

Director de la Tesis:

Dr. Moisés Santillán Zerón

Apodaca, Nuevo León — Junio, 2017

CENTRO DE INVESTIGACIÓN Y DE ESTUDIOS AVANZADOS
DEL INSTITUTO POLITÉCNICO NACIONAL
UNIDAD MONTERREY

A Mathematical Model for Calcium Release Via Ryanodine Receptors and Calcium-Calsequestrin Dynamics in Smooth Muscle Cells

Thesis presented by

Laura Sánchez Gómez

submitted for the degree of

Master of Science

in

Biomedical Engineering and Physics

Thesis Advisor:

Moisés Santillán Zerón Ph.D.

Apodaca, Nuevo León June, 2017

A Leis, por haberse embarcado
en esta maravillosa avetura
conmigo.

Acknowledgments

Al Dr. Moisés Santillán por su dirección y conocimientos pues me permitió encontrar un lugar en la investigación que es a la vez desafiante y gratificante; y por haber dispuesto un espacio en el cual expresarme libremente.

A los Drs. Daniel Sánchez y Jesús Rodríguez por tener siempre sus oficinas abiertas y todos sus valiosos aportes a este trabajo.

A mi familia y amigos por su apoyo incondicional y por esperarme siempre con los brazos abiertos.

Al Gordi, Albert, Isa, Mauro, Karina y Franco por haber sido mi familia y mi piso mientras estuve aquí.

A Saúl por haber tenido la disposición, la paciencia y por presionarme siempre para hacer mejor las cosas. A Yisus por oír sin queja todas mis teorías e ideas más locas cuando parecía que *python* había tirado la toalla.

A Cinvestav por haberme dado esta maravillosa oportunidad y a todos los docentes que hicieron parte del proceso.

A Conacyt por otorgarme la beca para realizar mis estudios.

Abbreviations

PMCA Pumps - Plasma Membrane Calcium Pumps.

SERCA Pumps - Sarcoplasmic/Endoplasmic Reticulum Calcium Pumps.

RyRs - Ryanodine Receptors.

IP_3Rs - Inositol 1,4,5-triphosphate Receptors.

ATP - Adenosine Triphosphate.

IP_3 - Inositol 1,4,5-triphosphate.

PIP_2 - Phosphatidylinositol 4,5-bisphosphate.

DAG - Diacylglycerol.

CICR - Calcium Induced Calcium Release.

$[Ca^{2+}]_i$ - Free Intracellular Calcium.

$[Ca^{2+}]_{SR}$ - Free Sarcoplasmic Reticulum Calcium.

KonD - Kinetics on Demand.

SK - Saturable Kinetics.

Tgn - Thapsigargin.

Caff - Caffeine.

Ca^{2+} - Calcium.

CSQ - Calsequestrin.

sCSQ - Rabbit Skeletal Muscle Calsequestrin.

cCSQ - Canine Cardiac Muscle Calsequestrin.

ΔC27 - Mutant Cardiac Calsequestrin.

M - Monomers.

D - Dimers.

T - Tetramers.

P - Polymers.

FO - Fractional Occupancy.

Variables and Parameters

$[Ca^{2+}]_i^T$— Total intracellular calcium (M).

$[Ca^{2+}]_{SR}^T$— Total sarcoplasmic reticulum calcium (M).

J_1— Flux via any removal mechanism located on the plasma membrane ($\mathrm{M\,s^{-1}}$).

J_2— Flux via ryanodine receptors ($\mathrm{M\,s^{-1}}$).

J_3— Flux via SERCA pumps ($\mathrm{M\,s^{-1}}$).

γ— Ratio between the cell volume and the sarcoplasmic reticulum volume (%).

a— First order kinetics constant, represents the removal rate via every removal mechanism in the plasma membrane ($\mathrm{s^{-1}}$).

$[Ca^{2+}]_i$— Free intracellular calcium (M).

$[\overline{Ca^{2+}}]_i$— Free basal intracellular calcium (M).

b— Maximum rate through one ryanodine receptor ($\mathrm{s^{-1}}$).

n_v— Fitting parameter (dimensionless).

$P\left([Ca^{2+}]_i, [Caff]\right)$ — Opening probability of a RyR depending on calcium concentration in the cytoplasm and applied caffeine concentration (dimensionless).

$[Caff]$— Caffeine concentration (M).

$[Ca^{2+}]_{SR}$— Free sarcoplasmic reticulum calcium (M).

$[\overline{Ca^{2+}}]_{SR}$— Free basal sarcoplasmic reticulum calcium (M).

$[S]$— Free ryanodine receptor subunit (M).

$[S]_T$— Total ryanodine receptor subunit (M).

$[S_{Ca}]$— Ryanodine receptor subunit bound to calcium (M).

$[S_{Caff}]$— Ryanodine receptor subunit bound to caffeine (M).

$[S_{CaCaff}]$— Ryanodine receptor subunit bound to calcium and caffeine (M).

k_F— Cooperativity between calcium and caffeine (dimensionless).

K_R— Dissociation constant of the complex RyR-calcium (dimensionless).

$K_{F'}$— Dissociation constant of the complex RyR-caffeine (dimensionless).

k_f— Quotient between k_F and $K_{F'}$ (dimensionless).

n_F— Hill coefficient that represents cooperativity among the RyR subunits (dimensionless).

c— Maximum flux through SERCA pumps ($\mathrm{M\,s^{-1}}$).

K_s— Half saturation constant of SERCA pumps (M).

n_s— Hill coefficient (dimensionless).

β— Binding capacity of the cytoplasm (dimensionless).

K_m— Half saturation constant of monomers (M).

M— Maximum concentration of calcium bound to monomers (M).

K_h— Half saturation constant of dimers (M).

D— Maximum concentration of calcium bound to dimers (M).

n— Hill coefficient (dimensionless).

p— Horizontal translation for Hill function (M).

q— Vertical translation for Hill function (M).

R_i for $0 \leq i \leq n$— Concentration of calsequestrin monomers with i bound calcium ions (M).

C— Free calcium concentration (M).

R_{D_j} for $0 \leq j \leq m$— Concentration of calsequestrin dimers with j additional bound calcium ions (M).

R_{T_k} for $0 \leq k \leq m$— Concentration of calsequestrin tetramers with k additional bound calcium ions (M).

K_c— Calcium-calsequestrin dissociation constant (M).

K_d— Calsequestrin polymerization constant (M).

FO— Fractional occupancy (dimensionless).

Resumen

Dentro de las células, el calcio tiene una dinámica antagónica y compleja. Por un lado, se utiliza para inducir y regular diferentes proceso, lo que implica que debe estar disponible; y por otro lado, altas concentraciones de calcio son citotóxicas. Por ello, la célula cuenta con compartimentos de almacenamiento de calcio como el retículo endoplásmico/sarcoplásmico. Para mantener los niveles de calcio, la célula hace uso de diferentes mecanismos. Por ejemplo, dentro del retículo se encuentran proteínas amortiguadoras que secuestran calcio. Esto permite que se almacenen grandes cantidades de calcio en el compartimento, mientras los niveles de calcio libre se mantienen bajos. Trabajos previos han descrito la cinética que hace posible esta gran capacidad amortiguadora en el retículo; sin embargo, violan los principios mismos de la biología. Nosotros desarrollamos un enfoque que explica y describe la cinética de interacción de calsecuestrina con calcio, teniendo en cuenta su capacidad para polimerizarse y lo incorporamos al modelo que describe la dinámica de liberación de calcio en células de músculo liso. Abordamos también la importancia de las bombas SERCA en la regulación de la liberación de calcio y realizamos un análisis de estabilidad para determinar la efectividad de nuestro enfoque en la recuperación de los niveles basales de calcio.

Abstract

Calcium presents a complex and antagonistic dynamics within the cell. On the one hand, it is widely used to induce and regulate different processes, which means calcium needs to be available; on the other hand, the excess of calcium is cytotoxic. As a solution, the cell has calcium storage compartments such as the endoplasmic/sarcoplasmic reticulum. In order to maintain calcium levels, the cell appeals to different mechanisms. For instance, inside the sarcoplasmic reticulum there are several binding proteins that sequester calcium. This allows the compartment to store high amounts of calcium, nevertheless free concentrations remain low. Attempts have been made to describe the kinetics of this high buffering capacity in the sarcoplasmic reticulum. However, they violate biology itself. We developed an approach that explains and describes calcium-calsequestrin kinetics considering its ability to polymerize and incorporated it to the mathematical model that describes calcium release in smooth muscle cells. We also tackled the importance of SERCA pumps in adjusting calcium release, and did a stability analysis to determine the effectiveness in restoring calcium basal concentration with our approach.

Contents

List of Figures

List of Tables

Introduction

Calcium is of great importance to cells. It participates in different processes such as proliferation, contraction, relaxation and apoptosis. As a second messenger, it transmits information from the surface of the cell to its interior. Calcium regulates such processes through different signaling mechanisms that depend on time, space and amplitude. Among them we find calcium sparks, in which intracellular calcium concentration increases for milliseconds; calcium transients that spread out in the cytoplasm and last for seconds; and calcium oscillations, which are periodic and complex global changes in intracellular calcium concentration and last for several seconds and in some cases minutes [1].

The excess of calcium in the cytoplasm is toxic. High concentrations of intracellular calcium produce protein and nucleic acids aggregation, jeopardizing the plasma membrane integrity that results in phosphates precipitation [1]. As a consequence, cells invest a lot of energy in maintaining free calcium levels in the cytoplasm around 100 nM. Since calcium cannot be chemically altered, cells must chelate, compartmentalize or extrude it. To do it, cells are provided with different mechanisms such as pumps, channels, exchangers and buffering proteins [2, 3].

Calcium accesses the cytoplasm from the extracellular space and from a compartment found inside cells called endoplasmic reticulum in non muscle cells and sarcoplasmic reticulum in muscle cells. Voltage and ligand dependent calcium channels in the plasma membrane introduce calcium to the cell, while sodium/calcium exchangers and PCMA pumps (Plasma Membrane Calcium ATPases) extrude it. Additionally, in the sarcoplasmic/endoplasmic reticulum membrane there are embedded calcium liberation channels such as RyRs (ryan-

odine receptors) and IP_3Rs (inositol 1,4,5-trisphosphate receptors); as well as SERCA pumps (Sarcoplasmic/Endoplasmic Reticulum Calcium ATPases) in charge of filling the reticulum. Furthermore, inside the sarcoplasmic/endoplasmic reticulum there are calcium binding proteins that work as buffers [4, 2]. Figure 1.

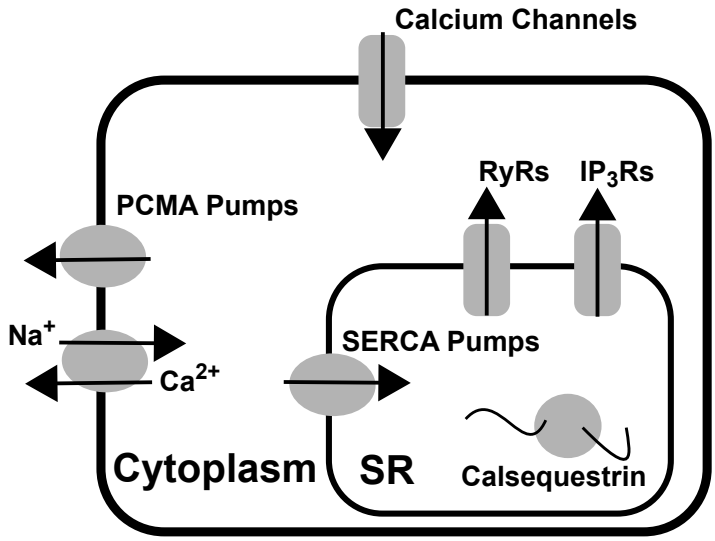

Figure 1: Graphical model of smooth muscle cells calcium mechanisms. Mechanisms involved in calcium release, recovery and storage within smooth muscle cells.

PMCA and SERCA pumps belong to the family of type P ATPases because they phosphorylate during transport. They have a transmembrane domain and a cytosolic domain with ATP hydrolysis and phosphorylation sites. The pumps have two conformational states, E1 and E2, and they go from one to the other during transport. E1 state is open to the cytoplasm and it is more stable when the protein is not phosphorylated, moment in which calcium bounds to it. E2 state is open to the extracellular space (in PCMA pumps) or to the interior of the sarcoplasmic/endoplasmic reticulum (in SERCA pumps); it is more stable when the protein is phosphorylated and calcium is released [2, 1].

As mentioned above, calcium release channels in the sarcoplasmic/endoplasmic reticulum are RyRs and IP_3Rs. IP_3Rs are activated by IP_3. IP_3 is produced by the following signaling cascade: in the plasma membrane there are muscarinic receptors, this receptors are coupled to a G protein. When the agonist binds the receptor, the G protein dissociates and

activates a phospholipase C that hydrolyzes PIP_2 (phosphatidylinositol 4,5-bisphosphate) to produce IP_3 and DAG (diglyceride). On the other hand, RyRs are activated by a process denominated CICR (Calcium Induced Calcium Release). An increase in intracellular calcium concentration above basal concentration is sensed by RyRs and calcium release from the sarcoplasmic/endoplasmic reticulum starts [5].

Inside the sarcoplasmic/endoplasmic reticulum there are different calcium binding proteins. Among them, calsequestrin: a high capacity and low affinity protein. Calsequestrin works as a buffer which allows the sarcoplasmic/endoplasmic reticulum to store high concentrations of calcium but maintaining the free luminal calcium concentration around 100 µM. When luminal calcium concentration is high enough, calsequestrin begins to polymerize forming dimers, then tetramers and finally polymers, increasing its binding capacity [6, 7]. Polymers of calsequestrin are formed by the interaction of either its amino-terminal segments denominated *front-to-front* polymerization, or its carboxyl-terminal segments denominated *back-to-back* polymerization [7]. Figure 2.

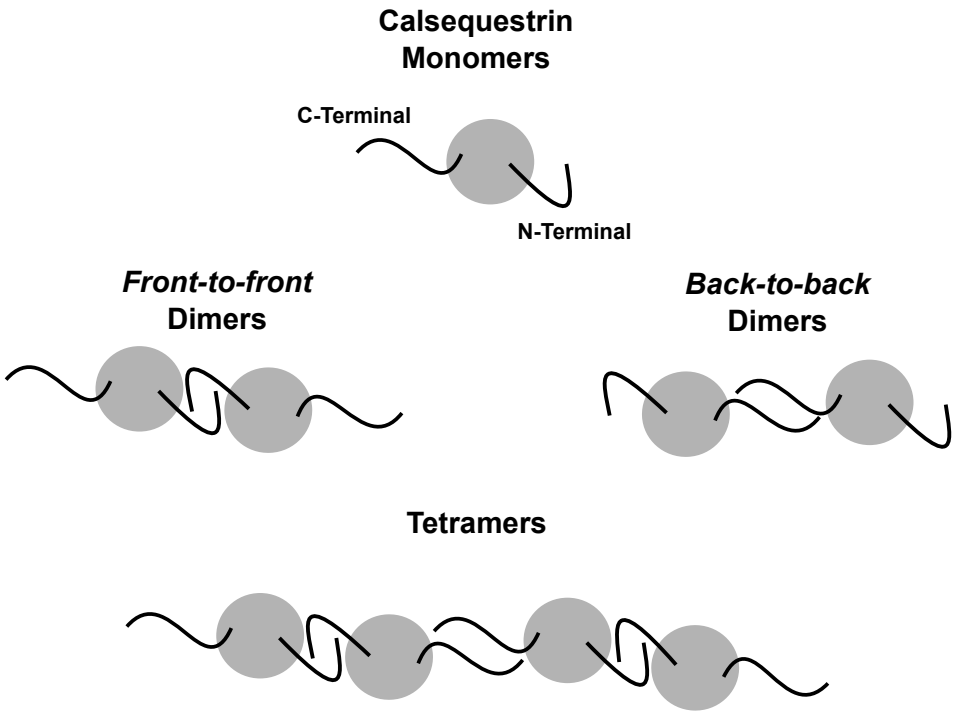

Figure 2: Graphical model of calsequestrin polymerization. Calsequestrin monomers, *front-to-front*, *back-to-back* dimers and tetramers.

Free calcium concentration in the cell compartments (cytoplasm and sarcoplasmic reticulum) can be quantified using calcium chelators that increase their fluorescence when they bind to it. The experiments mentioned here employed Fura-2 and Mag-Fluo4. Fura-2, which is used to measure free calcium concentration in the cytoplasm, is a fluorophore with high affinity for calcium ($K_d = 0.23\,\mu M$). It emits fluorescence when excited by two different wave lengths (340 nm and 380 nm), and this allows quantification of the amount of calcium bound to this chelator. Mag-Fluo4, used to measure free calcium concentration in the sarcoplasmic reticulum, is a low affinity calcium fluorophore (K_d =22 µM). It emits fluorescence when excited by one wave length (390 nm), therefore the amount of calcium is quantified in terms of the proportional increase of its fluorescence [8].

Chapter 1

Background

Different experiments have been performed to describe calcium dynamics inside cells when released from internal compartments. In smooth muscle cells isolated from guinea pig urinary bladder, Dagnino-Acosta *et al.* [9] observed that after stimulating with 20 mM of caffeine for 5 s, an increase in the free intracellular calcium, *i.e.* calcium in the cytoplasm ($[Ca^{2+}]_i$) produced a decrease in the free luminal calcium, *i.e.* calcium in the sarcoplasmic reticulum ($[Ca^{2+}]_{SR}$) as shown in figure 1.1. After 30 seconds, basal concentrations were recovered in both compartments. This suggests that calcium might be moving from one compartment to the other. However, after applying another equally-large (20 mM for 5 s) caffeine pulse, the reduction in the sarcoplasmic reticulum was similar, but the transient in the cytoplasm was smaller; which is counterintuitive. Since several minutes were needed to obtain a response similar to the one of the first pulse, it is possible to assume the existence of a refractory period in the sarcoplasmic reticulum. Furthermore, this refractory period is not correlated with the recovery of the reticulum basal calcium concentration [4].

Guerrero-Hernández *et al.* [4] plotted the phase-plane trajectories for each of the pulses above, to study what was happening in each compartment. Figure 1.2. They observed that the first and second pulses presented four stages. The first one shows an increase in the response of $[Ca^{2+}]_i$ without significant reduction of $[Ca^{2+}]_{SR}$. The second stage shows a reduction in $[Ca^{2+}]_{SR}$ without important changes in $[Ca^{2+}]_i$. The third phase shows the reduction in $[Ca^{2+}]_i$ response while $[Ca^{2+}]_{SR}$ remains almost constant. Finally during phase

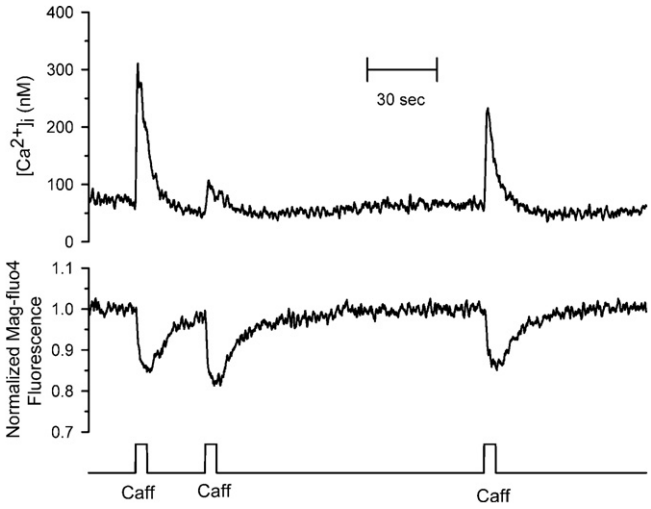

Figure 1.1: Calcium recovery in the sarcoplasmic reticulum. Simultaneous recording of $[Ca^{2+}]_i$ and $[Ca^{2+}]_{SR}$ in response to 5 seconds caffeine stimuli. Image retrieved from reference [9].

four there is a recovery in the $[Ca^{2+}]_{SR}$ with small changes in the $[Ca^{2+}]_i$. In contrast, the second pulse shows a linear behavior where phases one, two and three are lost. Due to this, the authors suggest that the sarcoplasmic reticulum has access to a concealed source of calcium, which is probably related to binding proteins. If calcium were just going from one compartment to the other, we would observe a linear behavior as shown in the second pulse. Furthermore, they propose that RyRs access bound calcium first rather than free calcium.

Using the same isolated cell type from the above experiment, Pérez-Rosas *et al.* [10] performed an experiment where calcium release was induced with 20 mM of caffeine for 5 seconds. Free calcium concentrations for both cytoplasm and sarcoplasmic reticulum were simultaneously recorded in time, as shown in figure 1.3A. After basal concentrations were recovered in both compartments, SERCA pumps were inhibited with 10 µM of thapsigargin for 5 seconds. After 20 seconds another 20 mM caffeine pulse was applied for 5 seconds. Phase-plane trajectories for each of the pulses are shown in 1.3B.

Figure 1.3A shows that thapsigargin did not altered basal levels of calcium in either compartment and as expected, luminal calcium concentration was not recovered after SERCA pumps were inhibited. However, although reduction in the luminal calcium was about the

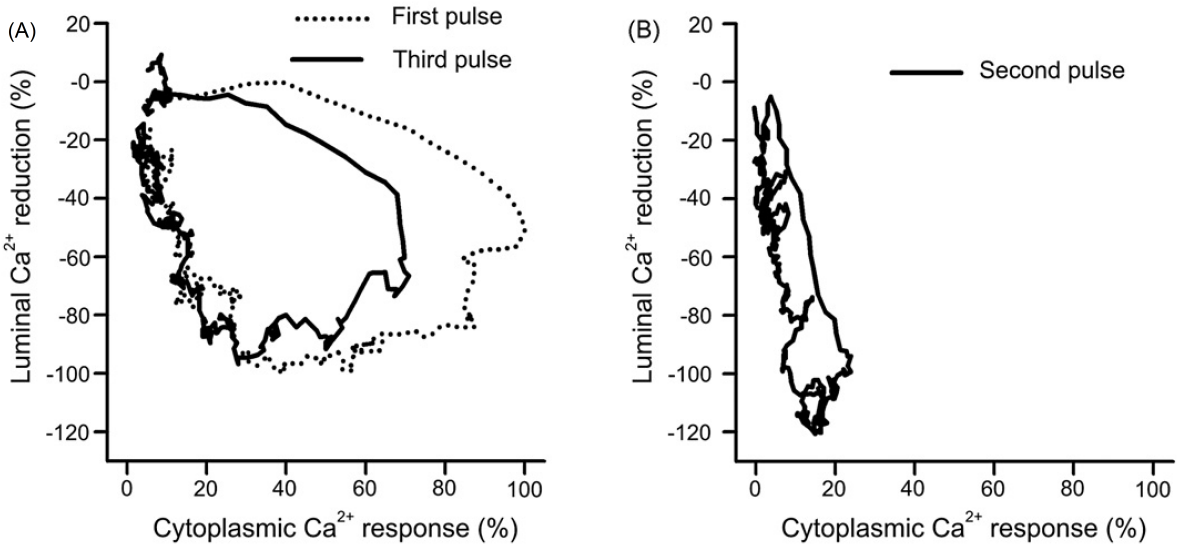

Figure 1.2: Smooth muscle cells calcium concentration phase-plane trajectories. The figure shows the phase planes of $[Ca^{2+}]_i$ versus $[Ca^{2+}]_{SR}$ for each of the caffeine pulses applied. Image retrieved from reference [4].

same, calcium transient after applying thapsigargin was smaller than that from the first pulse. Furthermore, calcium release stages in the second pulse were replaced by a unique phase presenting a linear behavior between the $[Ca^{2+}]_i$ increment and $[Ca^{2+}]_{SR}$ reduction (Figure 1.3). This suggests that SERCA pumps somehow intervene in calcium release from the sarcoplasmic reticulum.

Pérez-Rosas *et al.* [10] developed a mathematical model called Kinetics on Demand (KonD) to explain the above described counterintuitive situations observed experimentally. To that end, they focused on the buffering capacity of the calcium sequestering proteins in the sarcoplasmic reticulum. The model was constructed under the assumption that the kinetics of binding proteins was much more complex than what the authors refer to as Saturable Kinetics (SK). In SK, sequestering proteins such as calsequestrin have a finite number of binding sites. On the other hand, KonD suggests that the number of binding sites on buffering proteins increases as $[Ca^{2+}]_{SR}$ does. Consider the following reaction

$$[B_0] + [Ca^{2+}]_{SR} \underset{k_B^-}{\overset{k_B^+}{\rightleftharpoons}} [B_1], \tag{1.1}$$

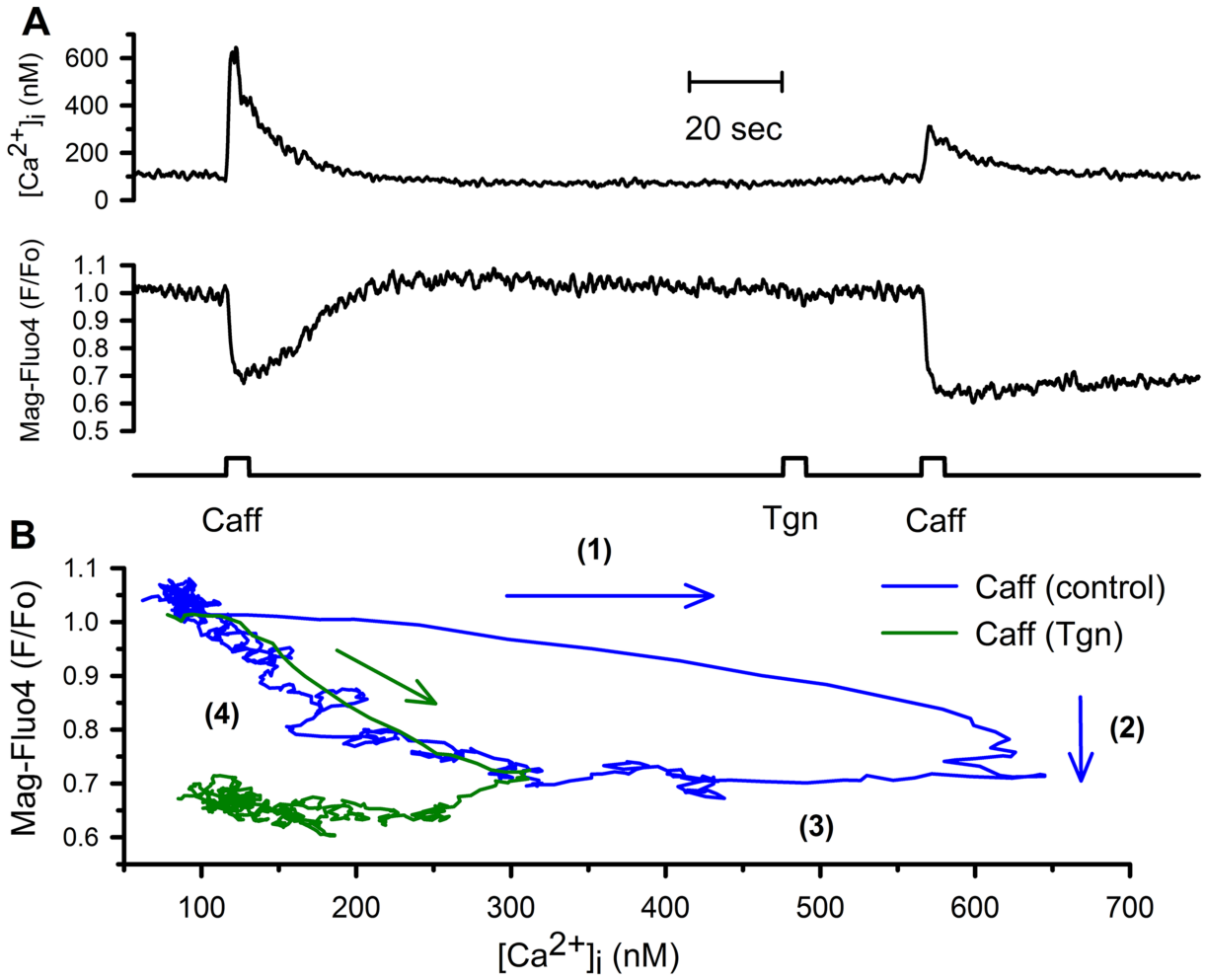

Figure 1.3: Caffeine-induced calcium release involve four phases that depend on SERCA pump activity. A. Time course of $[Ca^{2+}]_i$ and $[Ca^{2+}]_{SR}$. B. Phase planes for each of the caffeine pulses. Image retrieved from reference [10].

where $[B_0]$ represents the concentration of free calcium binding sites of calsequestrin and $[B_1]$ the concentration of filled binding sites. Analyzing the reaction in the equilibrium and by the law of mass action, that states that the ratio between the concentration of reactants and products is constant, they obtain

$$\frac{[B_0][Ca^{2+}]_{SR}}{[B_1]} = K_B, \tag{1.1}$$

with $K_B = \frac{k_B^-}{k_B^+}$ the dissociation constant of the reaction. In KonD model, the increment of binding sites was represented by the following equation in which $[B_T]$ is the total concentra-

tion of binding sites,

$$[B_0] = [B_T] + [B_1]. \tag{1.2}$$

Equation (1.2) implies that as long as luminal calcium concentration increases, the number of binding sites will continue to increase as well. Whilst in SK model, binding sites were represented by

$$[B_0] = [B_T] - [B_1]. \tag{1.3}$$

Equation (1.3) states that although luminal calcium concentration increases, at some point, calsequestrin molecules will not be able to bind more calcium.

In SK model calsequestrin calcium binding sites are finite and eventually as the $[\mathrm{Ca}^{2+}]_{SR}$ increases, they become saturated. Additionally, when calcium is released via RyRs, binding sites are emptied and compete for calcium with RyRs (Figure 1.4B). On the other hand, KonD proposes that binding sites increase together with $[\mathrm{Ca}^{2+}]_{SR}$. Furthermore, when calcium dissociates from calsequestrin, binding sites disappear. Then there is no competition between RyRs and binding proteins in the sarcoplasmic reticulum (Figure 1.4A) [1].

Inside the sarcoplasmic reticulum, total calcium concentration ($[Ca^{2+}]^T_{SR}$) is either free or bound to buffering proteins as shown by the following equation

$$[Ca^{2+}]^T_{SR} = [Ca^{2+}]_{SR} + [B_1]. \tag{1.4}$$

From equations (1.1), (1.2) and (1.4) Pérez-Rosas *et al.* showed that $[\mathrm{Ca}^{2+}]_{SR}$ in KonD model in terms of total luminal calcium concentration is given by

$$[Ca^{2+}]_{SR} = \frac{1}{2}\xi - \frac{1}{2}\sqrt{\xi^2 - 4[Ca^{2+}]^T_{SR}K_B}, \tag{1.5}$$

with $\xi = [Ca^{2+}]^T_{SR} + [B_0] + K_B$. In an analogous way, from equations (1.1), (1.3) and (1.4)

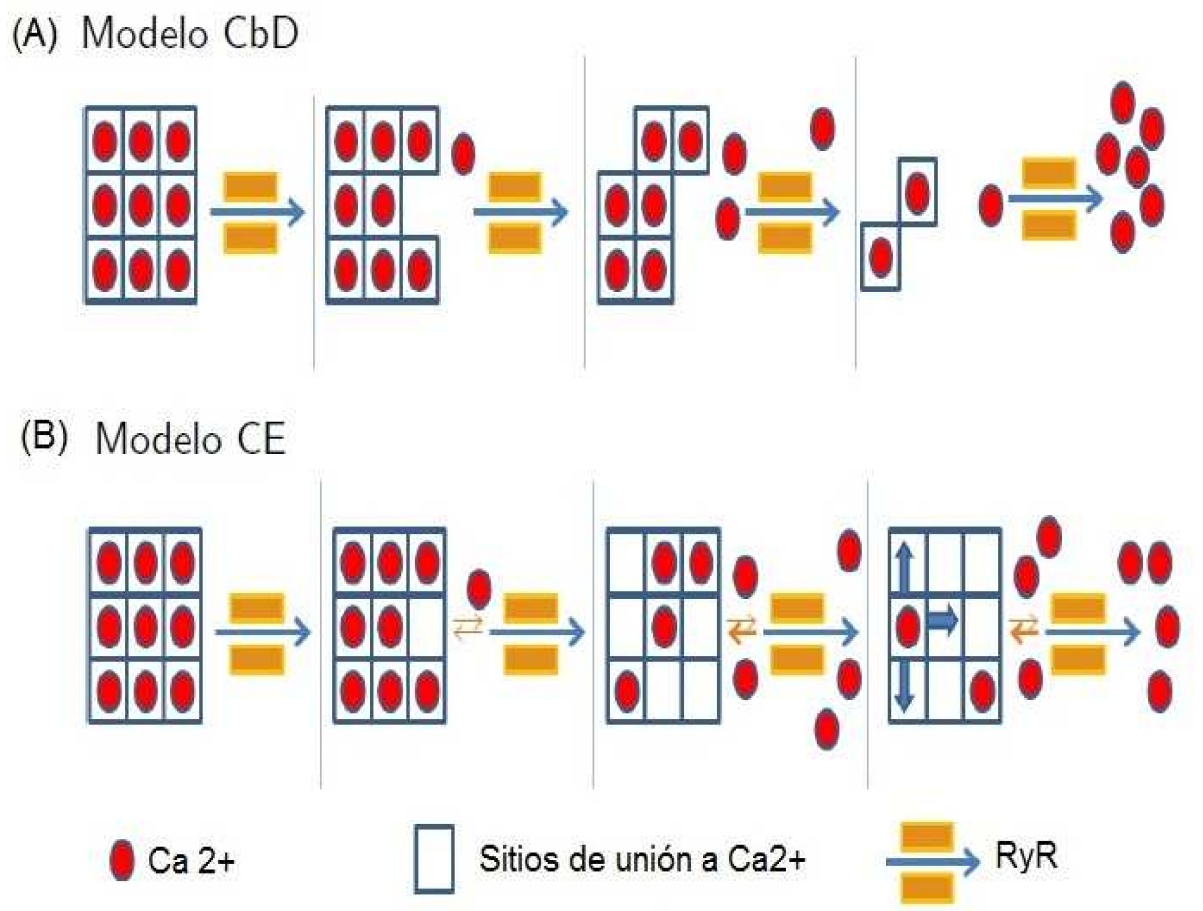

Figure 1.4: Calsequestrin calcium binding sites according to KonD and SK. A. According to KonD, binding sites appear and disappear when luminal calcium concentration increases or decreases, respectively. B. In SK there is a finite number of binding sites and they become saturated as luminal calcium concentration increases. Free binding sites compete with RyRs during calcium release. Image retrieved from reference [1].

for the SK model, $[\mathrm{Ca}^{2+}]_{SR}$ is given by

$$[Ca^{2+}]_{SR} = \frac{1}{2}\xi + \frac{1}{2}\sqrt{\xi^2 + 4[Ca^{2+}]^T_{SR}K_B}, \tag{1.6}$$

where $\xi = [Ca^{2+}]^T_{SR} - [B_0] - K_B$.

Figure 1.5 shows total vs free luminal calcium concentration plots for both SK and KonD models. In SK both total and free luminal calcium recover simultaneously. Since saturation of binding sites of calsequestrin in this kinetics is very slow, it implies that $[\mathrm{Ca}^{2+}]_{SR}$ recovery is slow as well. Conversely, KonD shows a quick recovery of $[\mathrm{Ca}^{2+}]_{SR}$. However, binding

starts almost as $[Ca^{2+}]_{SR}$ has been fully restored. As expected, there is no sign of saturation in this kinetics.

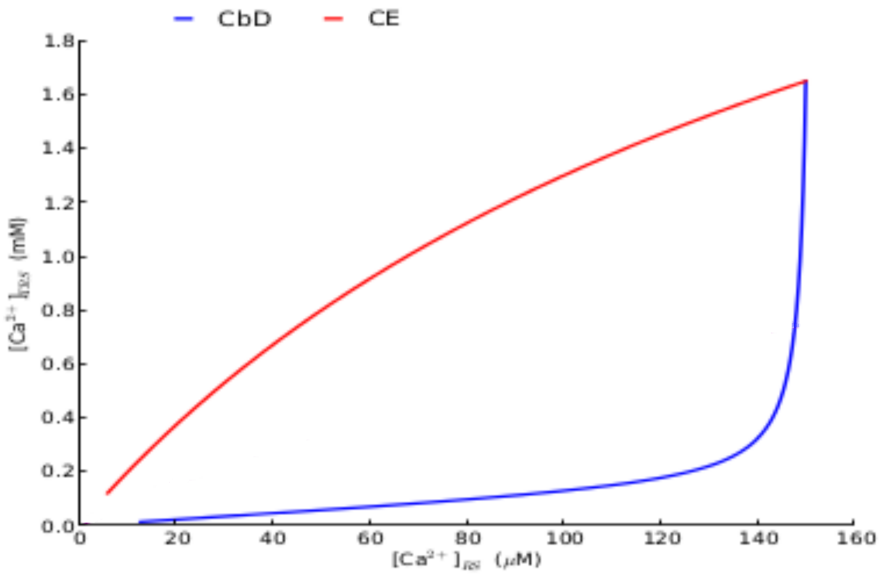

Figure 1.5: Total luminal calcium concentration vs free luminal calcium concentration for KonD and SK. Comparison between total luminal calcium concentration vs free luminal calcium concentration in SK model (red line) and KonD model (blue line). Image retrieved from reference [1].

Having established calsequestrin kinetics, it should be noted that Pérez-Rosas *et al.* fail to describe the mechanisms that allow calsequestrin to bind an extremely large amount of calcium. They incorporated this equations to the rest of the differential equations model they developed (described in section 3.1) and solved it numerically. To validate the model, they reproduced with it a 20 mM caffeine-induced experimental calcium transitory. Figure 1.6C shows the time course of $[Ca^{2+}]_i$ experimental data (circles) fitted by KonD model (blue line) and $[Ca^{2+}]_{SR}$ calculated with the model. Variability was simulated assuming that the volume of the sarcoplasmic reticulum varied from 1 % to 10 % of the cell volume. Figure 1.6A shows the rate of rise versus $[Ca^{2+}]_i$ response for 66 cells (dots), and data obtained with the model (blue line); in panel B the rate of rise versus rise time. Variability was modeled using the values of the parameters in the second column in table 1.1, while the transient was reproduced by making b =65 s^{-1} [1].

Parameter	20 mM Caff	2 mM Caff	20 mM Caff + 10 µM Tgn
a	$35\,s^{-1}$	$35\,s^{-1}$	$35\,s^{-1}$
b	$72.2\,s^{-1}$	$72.2\,s^{-1}$	$72.2\,s^{-1}$
c	$11.25\,\mu M\,s^{-1}$	$11.25\,\mu M\,s^{-1}$	$11.25\,\mu M\,s^{-1}$
$[Ca^{2+}]_i$	75 nM	75 nM	75 nM
γ	1 % to 10 %	1 % to 10 %	1 % to 10 %
n_v	1.7	1.7	1.7
K_s	300 nM	300 nM	300 nM
n_s	2	2	2
β	100	100	100
n_F	1.8	1.8	1.8
k_f	$4\,mM^{-1}$	$4\,mM^{-1}$	$0.3\,mM^{-1}$
$[Caff]$	20 mM	2 mM	20 mM
$[Ca^{2+}]^T_{SR_0}$	1.65 mM	1.65 mM	0.75 mM
$[\overline{Ca^{2+}}]_{SR}$	150 µM	150 µM	150 µM
K_B	151.1 µM	151.1 µM	151.1 µM
Tgn	0	0	1
CSQ	10	10	4

Table 1.1: KonD model parameters. Values of the parameters of the model developed by Pérez-Rosas. Data retrieved from reference [1].

To evaluate robustness of the model, Pérez-Rosas *et al.* reproduced an experimental 2 mM caffeine-induced pulse (figure 1.7C). For this pulse, the authors made RyRs relase slower by reducing their speed more than half (b =$35\,s^{-1}$) compared to the 20 mM transient, and increased cytoplasmic basal calcium concentration from 75 nM to 92.5 nM [1]. Variability for this transient was reproduced with values of the parameters in table 1.1 in the same way as for the 20 mM transient (figures 1.7A and 1.7B where experimental data for 49 cells were plotted).

To address the observed response after inhibiting SERCA pumps with 10 µM of thapsi-

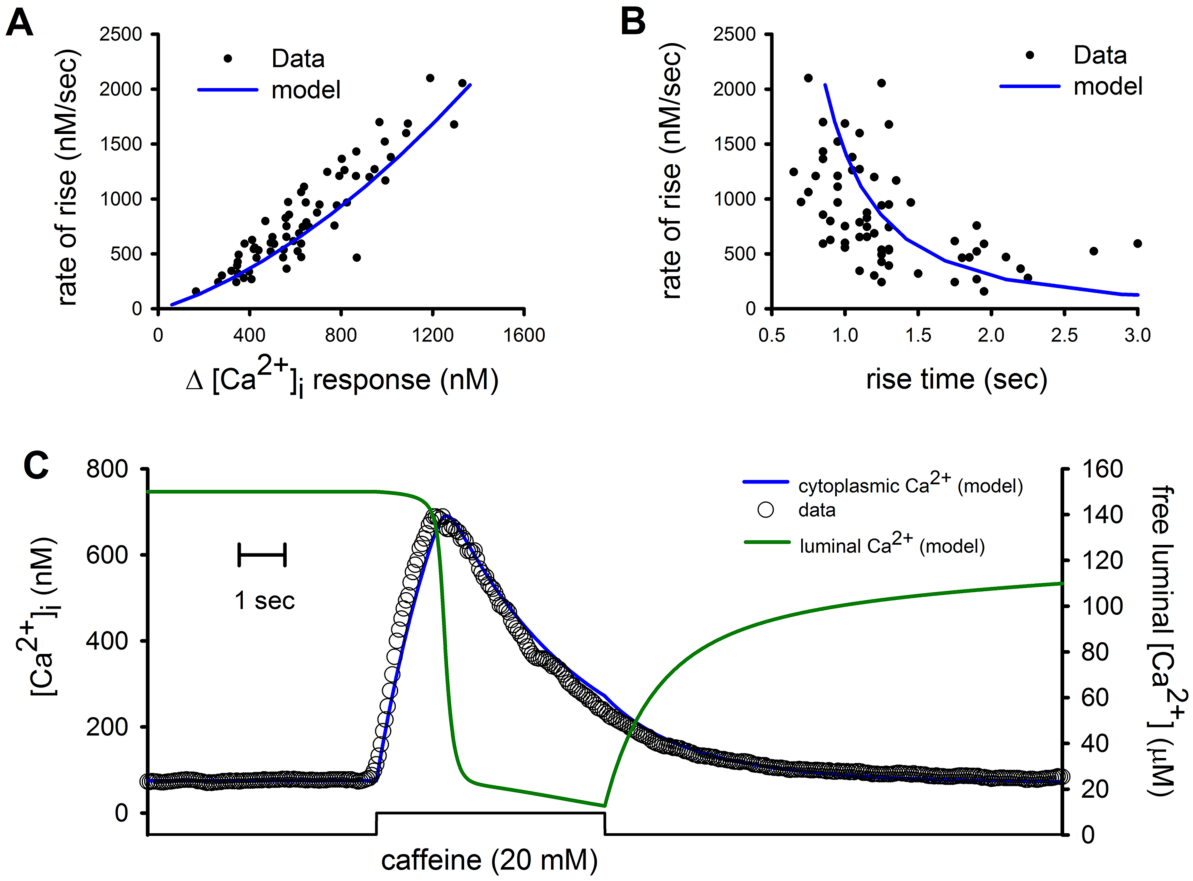

Figure 1.6: 20 mM caffeine-induced calcium response and fitting by KonD model. A. Variability of rate of rise versus $[Ca^{2+}]_i$ response. B. Rate of rise versus rise time. C. Time course of $[Ca^{2+}]_i$, fitting of KonD model and reduction of $[Ca^{2+}]_{SR}$. Image retrieved from reference [10].

gargin and applying 20 mM of caffeine, Pérez-Rosas *et al.* proposed that calsequestrin shifts from KonD to SK (figure 1.8). However, the mechanisms to explain this were not tackled. With this assumption and by changing several parameters (table 1.1) including cytoplasmic calcium basal concentration to 79.5 nM, Pérez-Rosas *et al.* reproduced the calcium transient (figure 1.6C) [1]. Values of the parameters for variability plots for 12 cells (figures 1.6A and 1.6B) can be found on table 1.1.

Pérez-Rosas *et al.* also simulated with both KonD and SK models the refractory period described by Guerrero-Hernández *et al.* [4]. SK model (green line) was not able reproduce neither the three cytoplasmic responses or the recovery in the sarcoplasmic reticulum (experimental data in red). KonD model (blue line) follows calcium recovery in the sarcoplasmic

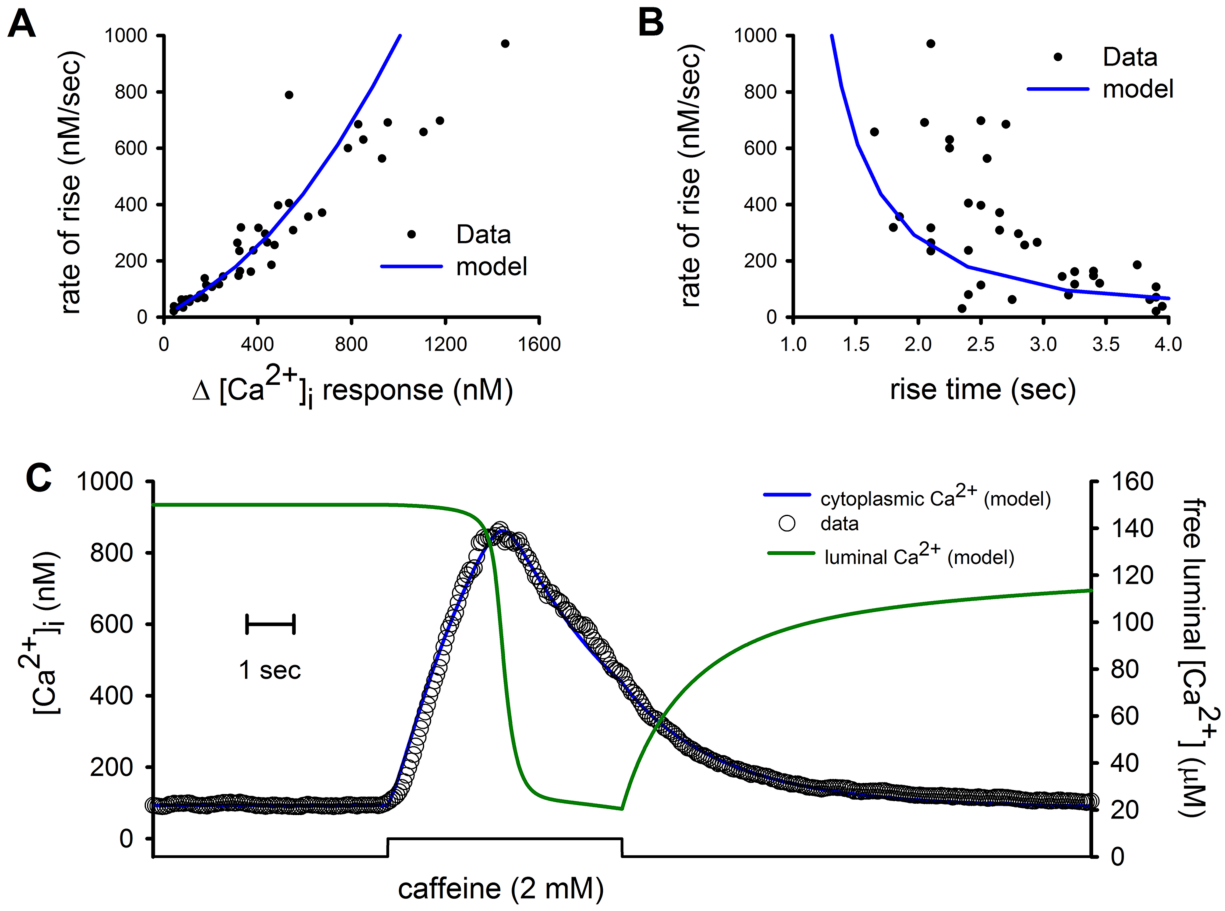

Figure 1.7: 2 mM caffeine-induced calcium response and fitting by KonD model. A. Variability of rate of rise versus $[Ca^{2+}]_i$ response. B. Rate of rise versus rise time. C. Time course of $[Ca^{2+}]_i$, fitting of KonD model and reduction of $[Ca^{2+}]_{SR}$. Image retrieved from reference [10].

reticulum but could not reproduce the last transient. Figure 1.10.

In summary, Pérez-Rosas *et al.* model was aimed at explaining the counterintuitive behavior observed experimentally in the sarcoplasmic reticulum. To do it, they focused on the buffering capacity of the compartment given by calcium sequestering proteins such as calsequestrin. However, although their model reproduced almost every set of data obtained experimentally, it has some issues. First of all, as previously mentioned, the number of binding sites of calsequestrin is an increasing function of calcium concentration. Moreover, the relationship is exponential (figure 1.11). This suggests that every time a binding site fills up, two new sites appear, so there is no saturation. Besides, for this to happen, a very

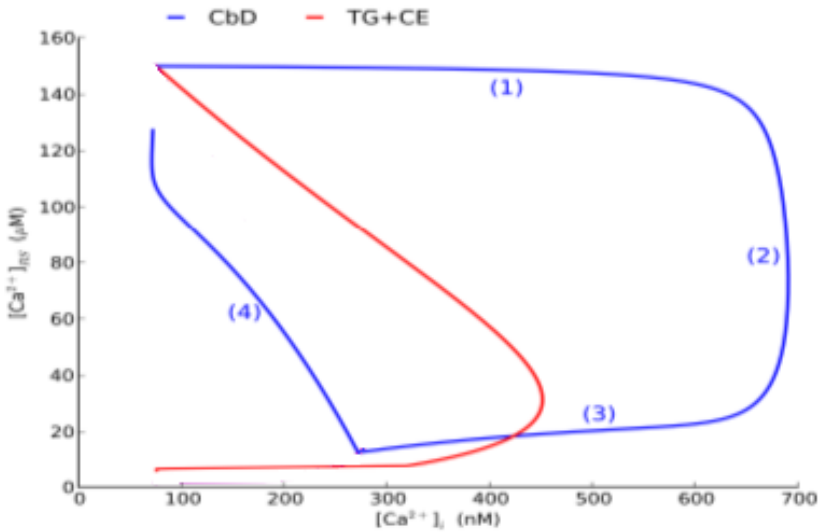

Figure 1.8: Phase-plane trajectories for KonD and SK models. Phase-plane trajectories for both KonD model (blue line) where the four stages of calcium release are shown and SK model (red line) after applying thapsigargin where stages disappear. Image retrieved from reference [10].

large number of binding sites will have to appear, which is not physically possible. Second, there is no explanation on what mechanisms allow calsequestrin to be a binding protein with infinitely large buffering capacity, nor why when SERCA pumps are inhibited suddenly it shifts its kinetics into a saturable one. And third, in order to reproduce every transient, the authors needed to modify one or several values of the parameters without apparent reason. Considering this issues we reviewed the literature to find if there were any experiments available that provided a different approach.

Park *et al.* [7] studied the relationship between calcium-calsequestrin binding and calsequestrin oligomerization. Experiments were done using rabbit skeletal muscle calsequestrin (sCSQ), canine cardiac muscle calsequestrin (cCSQ) and a mutant calsequestrin($\Delta C27$). The latter was the result of deleting the last 27 residues to the cardiac calsequestrin, affecting its way of polymerizing. To quantify calcium, authors used atomic absorption spectroscopy. Results are shown in figure 1.12. They observed that sCSQ presents a higher binding capacity than cCSQ, and $\Delta C27$ has a lower binding capacity than its wild type (over 50 %). Besides, the behavior of wild types varies depending on the concentration of calcium administered. As calcium increases, binding capacity increases as well. Furthermore, the Scatchard-type plot

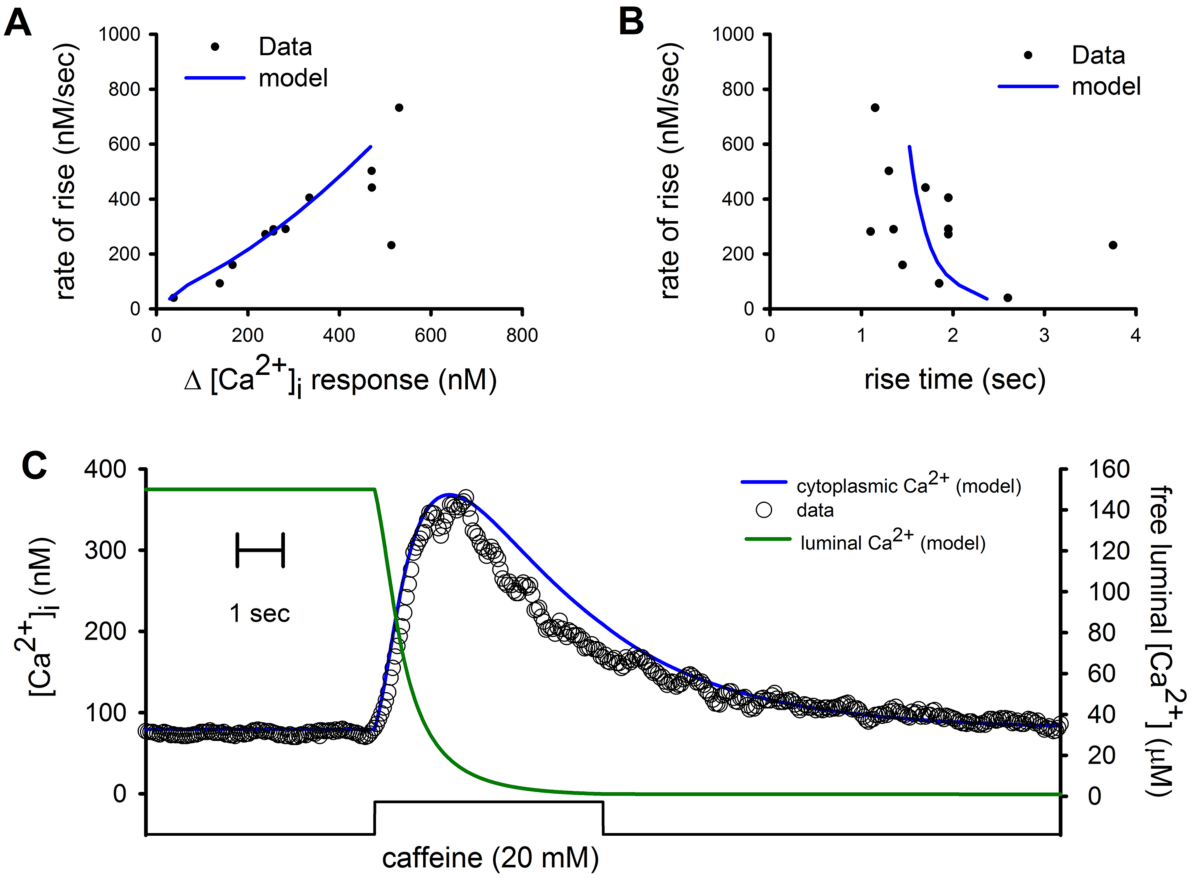

Figure 1.9: Effect of SERCA pump inhibition by thapsigargin on 20 mM caffeine-induced calcium responses and fitting by KonD model. A. Variability of rate of rise versus $[Ca^{2+}]_i$ response. B. Rate of rise versus rise time. C. Time course of $[Ca^{2+}]_i$, fitting of KonD model and reduction of $[Ca^{2+}]_{SR}$. Image retrieved from reference [10].

1.13 shows how the calcium-calsequestrin dissociation constant (represented by the slope) changes, which suggest that calsequestrin kinetics is complex and switches depending of the level of polymerization. This results reinforce the fact that buffering capacity of the sarcoplasmic reticulum varies depending on $[Ca^{2+}]_{SR}$ as described by Guerrero-Hernández *et al.* [4].

Calsequestrin polymerizes either *back-to-back* or *front-to-front*. However, since the last 27 residues were deleted from the mutant calsequestrin, it was forced to do it *front-to-front*. Due to this, $\Delta C27$ could only form dimers, but could not keep polymerizing, while wild types could. This observations suggest that there is a relationship between large binding capacity of calsequestrin and its oligomerization [7]. Figure 1.14 shows binding capacity of

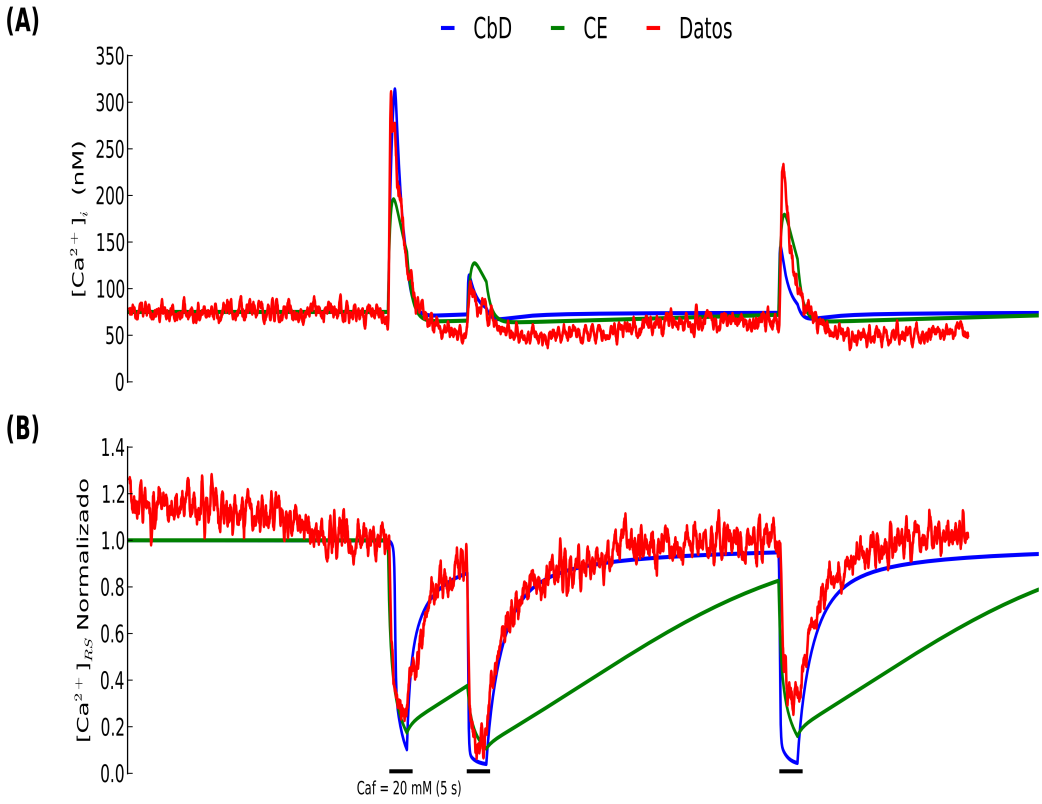

Figure 1.10: Caffeine-induced calcium release refractory response, fitting by KonD and SK model. The figure shows transients induced by caffeine, experimental data and fitting with SK and KonD models. Image retrieved from reference [1].

cCSQ (blue line) and sCSQ (red line) when found as monomers (M), dimers (D), tetramers (T) and polymers (P) against calcium concentration. Moreover, we can deduce that calcium concentration induces polymerization given that it begins for both wild types at the same point.

Taking Park *et al.* experiments into account, we wondered ourselves if it was possible to: first, reproduce in silico the behavior given calsequestrin polymerization; and second, incorporate it to the model. To that end we propose that calsequestrin has a fixed number of binding sites. However, when it polymerizes, additional calcium ions get trapped in the process. Therefore, its binding capacity increases as $[Ca^{2+}]_{SR}$ raises and polymerization takes place.

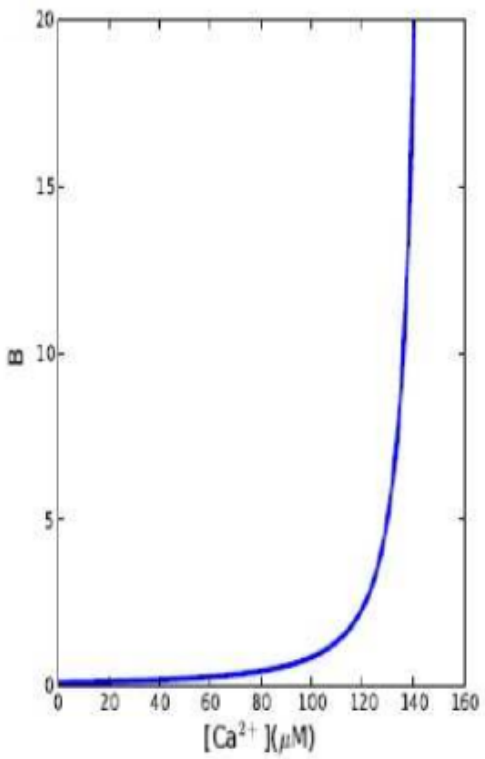

Figure 1.11: Buffering capacity versus luminal calcium concentration. Buffering capacity is an increasing function of $[Ca^{2+}]_{SR}$. Image retrieved from reference [1].

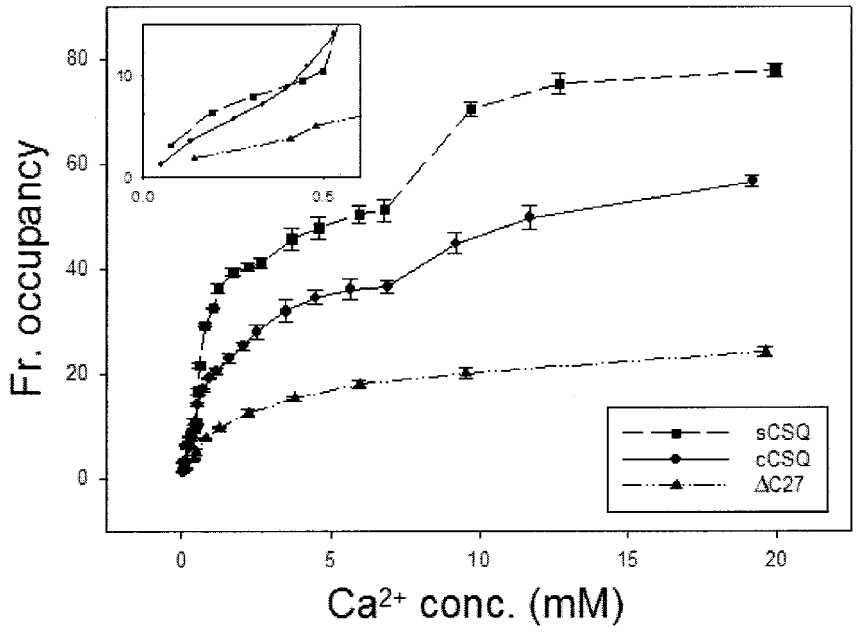

Figure 1.12: Calsequestrin oligomerization. Fractional occupancy (quotient of bound calcium concentration and total calsequestrin concentration) for polymers of wild type proteins sCSQ, cCSQ and dimers of mutant protein $\Delta C27$. The inset shows data for 0 mM to 0.5 mM. Image retrieved from the reference [7].

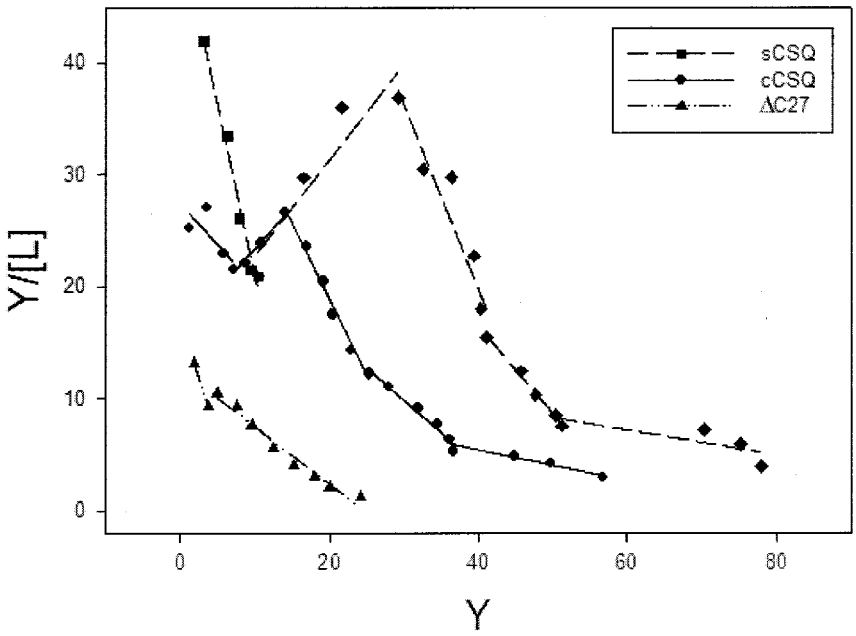

Figure 1.13: Scatchard-type plot for calcium-calsequestrin binding. Variation of calcium - calsequestrin dissociation constants. Image retrieved from reference [7].

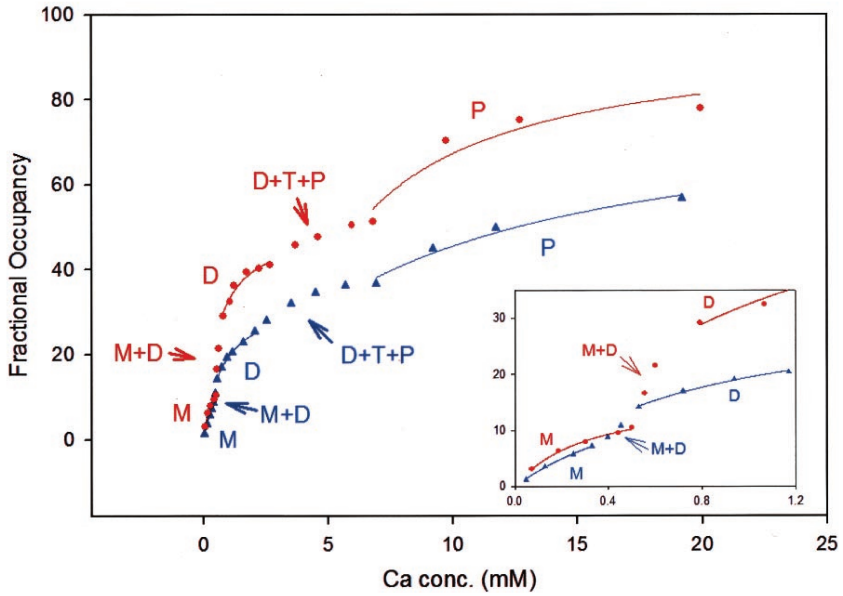

Figure 1.14: Calsequestrin monomers, dimers, tetramers and polymers. Bound calcium concentration when calsequestrin forms monomer (M), dimers (D), tetramers (T) and polymers (P). The inset shows data for 0 mM to 1.2 mM. Image retrieved from reference [7].

Chapter 2

Hypothesis and Objectives

Several experiments have shown that calcium release dynamics from the sarcoplasmic reticulum in smooth muscle cells is much more complex than previously thought. A mathematical model approach by Pérez-Rosas *et al.* [10] formulated a hypothesis to explain such behavior. Based on experiments by Park *et al.* [7] we formulated an alternative hypothesis.

2.1 Hypothesis

The kinetics of calcium-calsequestrin interaction and its polymerization, explain the counterintuitive behavior of the sarcoplasmic reticulum in smooth muscle cells.

2.2 General Objective

To analyze calcium dynamics when released via RyRs in smooth muscle cells, taking into account calsequestrin polymerization kinetics.

2.3 Specific Objectives

- To study calsequestrin calcium-dependent polymerization kinetics.
- To study calcium dynamics in smooth muscle cells via a mathematical modeling approach.

Chapter 3

Methodology

Pérez-Rosas *et al.* [10] developed a model to describe calcium release dynamics in the sarcoplasmic reticulum of smooth muscle cells, based on the function of binding proteins such as calsequestrin. However, although their model describes in great measure what happens during calcium release and recovery, the hypothesis on which the model is built cannot be physically sustained. Our approach was to complement such model, considering an important feature of calsequestrin as a buffering protein. The ability of calsequestrin to polymerize has proved experimentally to be the key of its large buffering capacity.

3.1 Model Development

The following model is based on the model developed by Pérez-Rosas *et al.* [10]. Lets assume smooth muscle cells as consisting of two compartments, the cytoplasm and the sarcoplasmic reticulum. We will study changes in the total calcium concentration in each compartment in terms of the net flux, *i.e.* the difference between input and output fluxes as shown in figure 3.1:

$$\begin{aligned} \frac{d[Ca^{2+}]_i^T}{dt} &= -J_1 + J_2 - J_3, \\ \frac{d[Ca^{2+}]_{SR}^T}{dt} &= \frac{J_3 - J_2}{\gamma}. \end{aligned} \tag{3.1}$$

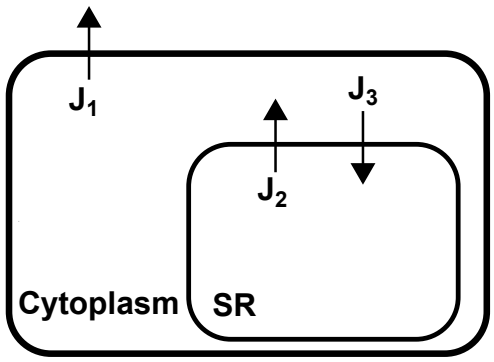

Figure 3.1: Graphical model of smooth muscle cells. Compartments (not at scale) and calcium fluxes of interest.

J_1 denotes the flux via any removal mechanism located in the plasma membrane, *e.g.* exchangers and PMCA pumps. Guerrero *et al.* proved that the removal process has a first order kinetics and therefore it will be given by

$$J_1 = a\left[[Ca^{2+}]_i - [\overline{Ca^{2+}}]_i\right], \tag{3.2}$$

where a is the first order kinetic constant and represents the removal rate, $[Ca^{2+}]_i$ is the free intracellular calcium concentration and $[\overline{Ca^{2+}}]_i$ is the basal concentration of free calcium in the cytoplasm.

J_2 represents the flux via RyRs and will be represented by

$$J_2 = b\gamma^{n_v} P\left([Ca^{2+}]_i, [Caff]\right)\left[[Ca^{2+}]_{SR} - [Ca^{2+}]_i\right], \tag{3.3}$$

with b a constant parameter proportional to the maximum flux through one RyR; γ is the ratio between cell volume and sarcoplasmic reticulum volume, and n_v is a fitting parameter, that accounts for the relation between the reticulum volume and the surface. Assuming that the density of RyRs is constant, the amount of them will be proportional to γ^{n_v}; $P\left([Ca^{2+}]_i, [Caff]\right)$ is the opening probability of a RyR and depends on free calcium in the cytoplasm and applied caffeine concentration; and $[Ca^{2+}]_{SR}$ is the free luminal calcium concentration. To derive P consider that each RyR is built up by four subunits. Assume that each subunit has one calcium and one caffeine binding sites. Let S denote the free subunit,

S_{Ca} represents a subunit bound by calcium, S_{Caff} a subunit bound by caffeine and S_{CaCaff} a subunit bound by both molecules. Furthermore, lets assume there is cooperativity between calcium and caffeine (k_F).

The following reactions represent the transitions between states of the subunits

$$[S] + [Ca^{2+}]_i \underset{k_R^-}{\overset{k_R^+}{\rightleftharpoons}} [S_{Ca}], \tag{3.1}$$

$$[S_{Ca}] + [Caff] \underset{k_{F'}^-}{\overset{k_F k_{F'}^+}{\rightleftharpoons}} [S_{CaCaff}], \tag{3.2}$$

$$[S] + [Caff] \underset{k_{F'}^-}{\overset{k_{F'}^+}{\rightleftharpoons}} [S_{Caff}], \tag{3.3}$$

$$[S_{Caff}] + [Ca^{2+}]_i \underset{k_R^-}{\overset{k_F k_R^+}{\rightleftharpoons}} [S_{CaCaff}]. \tag{3.4}$$

Analyzing the reactions in the equilibrium and by the law of mass action, obtain from reaction (3.1) that

$$[S_{Ca}] = \frac{[S][Ca^{2+}]_i}{K_R}, \tag{3.4}$$

where $K_R = \frac{k_R^-}{k_R^+}$. From reaction (3.2),

$$[S_{CaCaff}] = k_F \frac{[S_{Ca}][Caff]}{K_{F'}}, \tag{3.5}$$

with $K_{F'} = \frac{k_{F'}^-}{k_{F'}^+}$. From reaction (3.3),

$$[S_{Caff}] = \frac{[S][Caff]}{K_{F'}}, \tag{3.6}$$

and from reaction (3.4) they get that

$$[S_{CaCaff}] = k_F \frac{[S_{Caff}][Ca^{2+}]_i}{K_R}. \tag{3.7}$$

Substituting equation (3.4) into (3.5) and equation (3.6) in (3.7), we check that (3.5) and (3.7) are equivalent. Based on the principle of mass conservation, the total concentration of subunits is given by

$$[S]_T = [S] + [S_{Ca}] + [S_{Caff}] + [S_{CaCaff}]. \tag{3.8}$$

Replacing the concentrations in terms of $[S]$, $[Ca^{2+}]_i$ y $[Caff]$,

$$[S]_T = [S] + \frac{[S][Ca^{2+}]_i}{K_R} + \frac{[S][Caff]}{K_{F'}} + k_F \frac{[S][Ca^{2+}]_i[Caff]}{K_{F'}K_R}. \tag{3.9}$$

We are interested in the state in which calcium is bound to the subunits whether caffeine is bound or not, hence

$$\frac{[S_{Ca}] + [S_{CaCaff}]}{[S]_T} = \frac{\frac{[S][Ca^{2+}]_i}{K_R} + k_F \frac{[S][Ca^{2+}]_i[Caff]}{K_{F'}K_R}}{[S] + \frac{[S][Ca^{2+}]_i}{K_R} + \frac{[S][Caff]}{K_{F'}} + k_F \frac{[S][Ca^{2+}]_i[Caff]}{K_{F'}K_R}}. \tag{3.10}$$

Simplifying by $[S]$ and factoring $\frac{[Ca^{2+}]_i}{K_R}$ they obtain

$$\frac{[S_{Ca}] + [S_{CaCaff}]}{[S]_T} = \frac{\frac{[Ca^{2+}]_i}{K_R}\left(1 + k_F \frac{[Caff]}{K_{F'}}\right)}{1 + \frac{[Ca^{2+}]_i}{K_R}\left(1 + k_F \frac{[Caff]}{K_{F'}}\right) + \frac{[Caff]}{K_{F'}}}. \tag{3.11}$$

Suppose $K_F > 1$, $\frac{[Caff]}{K_{F'}} << 1$ and $k_f = \frac{k_F}{K_{F'}}$, equation (3.11) is now

$$\frac{[S_{Ca}] + [S_{CaCaff}]}{[S]_T} = \frac{[Ca^{2+}]_i\,(1 + k_f[Caff])}{K_R + [Ca^{2+}]_i\,(1 + k_f[Caff])}. \tag{3.12}$$

To induce the opening of RyRs there must be calcium bound to each of the subunits. Since there is cooperativity between the subunits [11], P can be rewritten as

$$P\left([Ca^{2+}]_i, [Caff]\right) = \frac{\left([Ca^{2+}]_i\,(1 + k_f[Caff])\right)^{n_F}}{K_R^{n_F} + \left([Ca^{2+}]_i\,(1 + k_f[Caff])\right)^{n_F}}, \tag{3.13}$$

where n_F is a Hill coefficient.

J_3 represents the flux via SERCA pumps into the sarcoplasmic reticulum. In [12] Lytton

et al. proved that this flux is described by the following Hill function

$$J_3 = c\frac{[Ca^{2+}]_i^{n_s}}{K_s^{n_s} + [Ca^{2+}]_i^{n_s}}, \tag{3.14}$$

with c the maximum flux through SERCA pumps, K_s the half saturation constant and n_s a Hill coefficient.

To relate free calcium concentrations with total calcium concentrations in each compartment, we will consider their buffering capacity. Most of the calcium that enters the cytoplasm binds to different binding proteins. There is experimental evidence that buffering capacity in this compartment is constant, due to the vast amount of buffers in it [13]. Binding capacity (β) will be given by the change in free cytoplasmic calcium due to a change in the total cytoplasmic calcium [14]

$$\beta = \frac{d[Ca^{2+}]_i^T}{d[Ca^{2+}]_i}, \tag{3.15}$$

When changes are small enough, the expression above can be substituted by

$$\beta = \frac{\Delta[Ca^{2+}]_i^T}{\Delta[Ca^{2+}]_i}. \tag{3.16}$$

The main purpose of our work was to represent calcium in the sarcoplasmic reticulum by considering calsequestrin polymerization as described by Park *et al.* in [7]. To do so, we reproduced their experimental data as described in section 4.1. However, results were rather complex and it was numerically inefficient to incorporate them to the model. For this reason, we needed an approximation of the overall behavior of the system observed by Park *et al.* without considering in detail how do the species interact. Furthermore, the total calcium concentration within the sarcoplasmic reticulum is around 1.6 mM. It was found experimentally that calsequestrin dimerizes from 0 mM to 1 mM and tetramers start to form after 3 mM [7, 15]. Considering these aspects, we used a combination of Hill equations (being a Michaelis-Menten equation a particular case with $n = 1$) which are widely used to describe biological processes as discussed by Santillán in [11]. As a result, free luminal calcium will

be represented by the following Michaelis-Menten and Hill inverse functions

$$[Ca^{2+}]_{SR} = \begin{cases} K_m \frac{[Ca^{2+}]^T_{SR}}{M-[Ca^{2+}]^T_{SR}} & \text{for} \quad [Ca^{2+}]^T_{SR} \leq p \\ K_h \left[\frac{[Ca^{2+}]^T_{SR}-p}{D-\left([Ca^{2+}]^T_{SR}-p\right)} \right]^{1/n} + q & \text{for} \quad [Ca^{2+}]^T_{SR} > p \end{cases}, \tag{3.17}$$

where K_m is the half saturation constant of monomers, M is the maximum concentration of calcium bound to monomers, K_h is the half saturation constant of dimers, D is the maximum concentration of calcium bound to dimers, n is a Hill coefficient, p and q are the horizontal and vertical translations, respectively.

3.2 Parameters Estimation

Parameter	**20 mM Caff**	**2 mM Caff**	**20 mM Caff + 10 µM Tgn**
β	100	100	100
K_m	5.5 µM	5.5 µM	5.5 µM
K_h	55 µM	55 µM	–
M	500 µM	500 µM	500 µM
D	2.8 mM	2.8 mM	–
n	3.9	3.9	–
p	472 µM	472 µM	–
q	94 µM	94 µM	–

Table 3.1: Free calcium functions parameters. Values of the parameters of $[Ca^{2+}]_i$ and $[Ca^{2+}]_{SR}$ functions.

Values of the parameters were based on those used by Pérez-Rosas *et al.* in their model [10]. However, we adjusted them in order to fit experimental data. Table 3.1 shows values of parameters specific to free calcium functions $[Ca^{2+}]_i$, $[Ca^{2+}]_{SR}$; table 3.2 shows values of parameters for the rest of the model. Both tables show the set of values that best reproduce each experiment.

Parameter	20 mM Caff	2 mM Caff	20 mM Caff + 10 µM Tgn
a	$33\,s^{-1}$	$33\,s^{-1}$	$33\,s^{-1}$
b	$71\,s^{-1}$	$71\,s^{-1}$	$71\,s^{-1}$
c	$9\,\mu M\,s^{-1}$	$9\,\mu M\,s^{-1}$	$9\,\mu M\,s^{-1}$
γ	6.1 %	7.5 %	14 %
K_R	≈233 nM	≈255 nM	≈333 nM
K_s	220 nM	220 nM	220 nM
k_f	$0.2\,mM^{-1}$	$0.2\,mM^{-1}$	$0.2\,mM^{-1}$
n_v	1.71	1.71	1.71
n_F	4	4	4
n_s	2	2	2
$[\overline{Ca^{2+}}]_i$	75 nM	75 nM	75 nM
$[\overline{Ca^{2+}}]_{SR}$	150 µM	150 µM	150 µM
$[Ca^{2+}]^T_{i_0}$	7.5 µM	7.5 µM	7.5 µM
$[Ca^{2+}]^T_{SR_0}$	1.65 mM	1.65 mM	482.3 µM
$[Caff]$	20 mM	2 mM	20 mM
Tgn	off	off	on

Table 3.2: General parameters. Values of the general parameters of the model that best fit experimental data. For figure 4.7 γ =2.5 % and K_R ≈156 nM. K_R is calculated by making $J_2 = J_3$, $[Caff] = 0$, $[Ca^{2+}]_i = [\overline{Ca^{2+}}]_i$ and $[Ca^{2+}]_{SR} = [\overline{Ca^{2+}}]_{SR}$ [1].

It is important to mention that the set of values was the same for every simulation presented on this thesis, except for those that changed in deliberately in the experiment (Tgn and $[Ca^{2+}]^T_{SR_0}$) and those related with the size of the cell (γ and K_R).

3.3 Model Validation

We acknowledge Agustín Guerrero Hernández Ph.D for providing us the experimental data to validate our model. Data presented here were published in [4] and [10].

Chapter 4

Results and Discussion

Considering the mathematical model developed by Pérez-Rosas *et al.* [10] and the experiments conducted by Park *et al.* [7], we developed an alternative hypothesis based on calsequestrin polymerization, to explain the ability of the sarcoplasmic reticulum to release large amounts of calcium, while simultaneously maintaining basal concentrations small enough to prevent stress. We present an explanatory, deterministic mathematical model. Simulations presented here are the result of solving the system of differential equations numerically with a fourth-order Runge-Kutta method implemented in *python*. Parameters used are found in tables 3.1 and 3.2.

4.1 Additional calcium binding during calsequestrin polymerization explains the increase in its buffering capacity

Our first approach was to reproduce experimental results by Park *et al.* [7] regarding the relationship between binding capacity and calsequestrin polymerization. To explain this relationship we proposed that additional calcium ions get trapped during polymerization. For the purpose of this work we considered only monomers, dimers and tetramers.

We assume that a monomer of calsequestrin can be bound by one calcium ion at a time

as shown in the following chain of reactions:

$$\begin{aligned} \mathrm{R_0 + C} &\rightleftharpoons \mathrm{R_1}, \\ \mathrm{R_1 + C} &\rightleftharpoons \mathrm{R_2}, \\ &\vdots \\ \mathrm{R_{n-1} + C} &\rightleftharpoons \mathrm{R_n}, \end{aligned}$$

where R_i for $0 \leq i \leq n$ represents the concentration of calsequestrin monomers with i bound calcium ions, while C is the free calcium concentration.

We further assume that when two monomers with all of their n binding sites occupied interact, they form a dimer

$$2\,\mathrm{R_n} \rightleftharpoons \mathrm{R_{D_0}},$$

where R_{D_0} represents the concentration of calsequestrin dimers. Although we initially considered that calcium ions get trapped during the dimerization, we needed an additional consideration in order to obtain the desired behavior. That is, the interaction of either C-terminal or N-terminal segments produces sort of a negatively charged pocket in which a finite number m of new binding sites appear. These new binding sites are filled one at a time as shown in the following reactions:

$$\begin{aligned} \mathrm{R_{D_0} + C} &\rightleftharpoons \mathrm{R_{D_1}}, \\ \mathrm{R_{D_1} + C} &\rightleftharpoons \mathrm{R_{D_2}}, \\ &\vdots \\ \mathrm{R_{D_{m-1}} + C} &\rightleftharpoons \mathrm{R_{D_m}}, \end{aligned}$$

where R_{D_j} for $0 \leq j \leq m$ is the concentration of calsequestrin dimers with j bound calcium ions.

After two dimers are full, they can interact to form a tetramer:

$$2\,\mathrm{R}_{\mathrm{D_m}} \rightleftharpoons \mathrm{R}_{\mathrm{T_0}},$$

with R_{T_0} the concentration of calsequestrin tetramers. The new interaction of either C-terminal or N-terminal segments can again give rise to m new binding sites, which are filled in the same way as they do in dimers. The process is shown in the following reactions

$$\begin{aligned}
\mathrm{R}_{\mathrm{T_0}} + \mathrm{C} &\rightleftharpoons \mathrm{R}_{\mathrm{T_1}}, \\
\mathrm{R}_{\mathrm{T_1}} + \mathrm{C} &\rightleftharpoons \mathrm{R}_{\mathrm{T_2}}, \\
&\vdots \\
\mathrm{R}_{\mathrm{T_{m-1}}} + \mathrm{C} &\rightleftharpoons \mathrm{R}_{\mathrm{T_m}},
\end{aligned}$$

where R_{T_k} for $0 \leq k \leq m$ represents the concentration of calsequestrin tetramers bound to k calcium ions. Figure 4.1 shows calcium bound and polymerization process according to the description above.

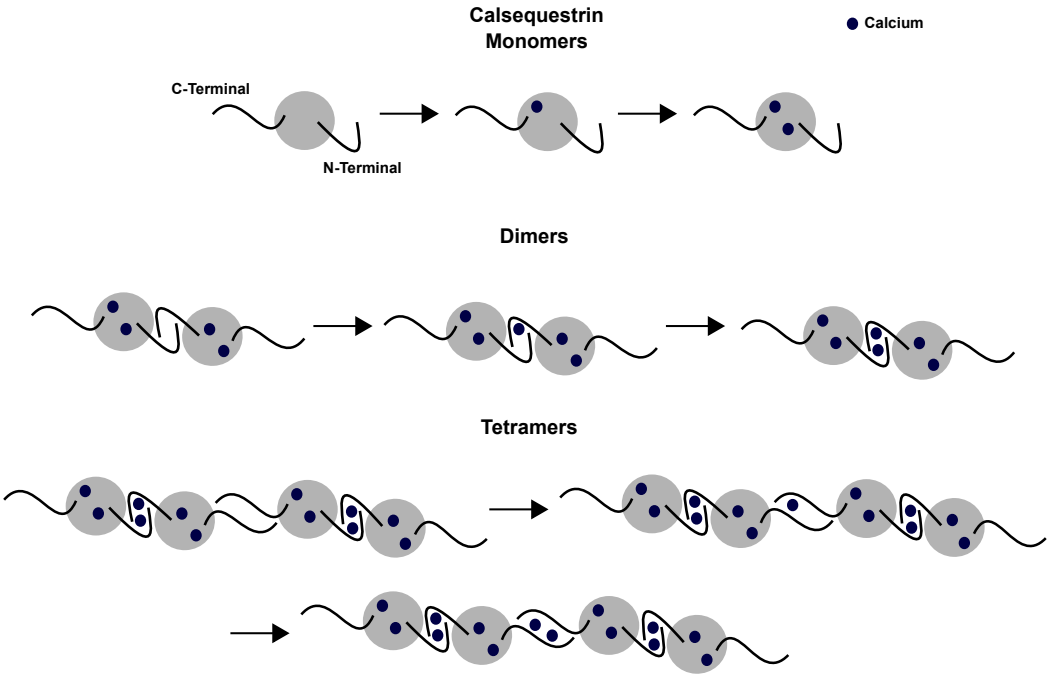

Figure 4.1: Calsequestrin calcium bound and polymerization process. Representation of calcium bound during polymerization assuming there are only two binding sites.

From the law of mass action the ordinary differential equations system accounting for the rate of change of all chemical species involved in the formerly described chemical reaction system is:

$$
\begin{cases}
\dot{R}_0 = K_c R_1 - n R_0 C, \\
\dot{R}_i = (n-i+1) R_{i-1} C - (n-i) R_i C + (i+1) K c R_{i+1} - i K_c R_i, & \text{for } 1 \le i \le n-1, \\
\dot{R}_n = R_{n-1} C - n K_c R_n + 2 K_d R_{D_0} - 2 R_n^2, \\
\dot{R}_{D_0} = R_n^2 - K_d R_{D_0} + K_c R_{D_1} - m R_{D_0} C, \\
\dot{R}_{D_j} = (m-j+1) R_{D_{j-1}} C - j K_c R_{D_j} + (j+1) K_c R_{D_{j+1}} - (m-j) R_{D_j} C, & \text{for } 1 \le j \le m-1, \\
\dot{R}_{D_m} = R_{D_{m-1}} C - m K_c R_{D_m} + 2 K_d R_{T_0} - 2 R_{D_m}^2, \\
\dot{R}_{T_0} = R_{D_m}^2 - K_d R_{T_0} + K_c R_{T_1} - m R_{T_0} C, \\
\dot{R}_{T_k} = (m-k+1) R_{T_{k-1}} C - k K_c R_{T_k} + (k+1) K_c R_{T_{k+1}} - (m-k) R_{T_k} C, & \text{for } 1 \le k \le m-1, \\
\dot{R}_{T_m} = R_{T_{m-1}} C - m K_c R_{T_m}
\end{cases}
$$

where K_c is the dissociation constant of the calcium-calsequestrin binding reaction and K_d is the dissociation constant for polymerization.

After numerically solving the above ordinary differential equations system for a long period of time (t =1000 *units*) in order for it to reach a steady state, we calculated the fractional occupancy (FO) with the following equation

$$FO = \sum_{i=0}^{n} i R_i + \sum_{j=0}^{m} (2n + j) R_j + \sum_{k=0}^{m} (2(2n+m) + k) R_k. \tag{4.1}$$

Results are shown in figure 4.2.

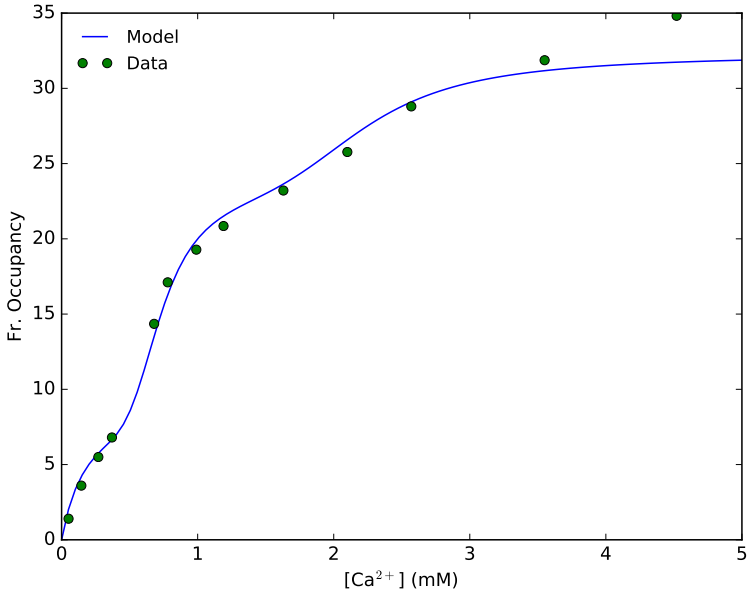

Figure 4.2: Binding capacity of calsequestrin monomers, dimers and tetramers. Green dots represent data replotted from figure 1.14 (Park *et al.* [7]), blue line obtained with parameters $n = 10$, $m = 30$, $K_c = 0.2\,\text{mM}$, $K_d = 300\,\text{mM}$ and $t = 1000$ units of time.

4.2 Calsequestrin polymerization kinetics fits 20 mM caffeine-induced calcium release

As mentioned in section 3.1, for the purpose of our model we are interested in the overall behavior of calsequestrin polymerization. Due to this and the fact that concentrations used in Park's *et al.* experiments are too high compared with those in cells, we approximated the latter result with a combination of Hill equations (equation (3.17)) as shown in figure 4.3.

Figure 4.4 shows the time course of the $[Ca^{2+}]_i$ response to a 20 mM caffeine stimulus (both experimental data (circles), data obtained *in silico* by numerically solving the model (red line)) and changes in $[Ca^{2+}]_{SR}$ derived from the model (blue line). In order to determine if the model allowed us to explain what happens during calcium release, we plotted pairs of the form $([Ca^{2+}]_i, [Ca^{2+}]_{SR})$ obtained for every value of time (t). From now on we will refer to these plots as phase planes or phase diagrams. As shown in figure 4.5, our model reproduces the four phases of calcium release observed by Guerrero-Hernández *et al.* [4].

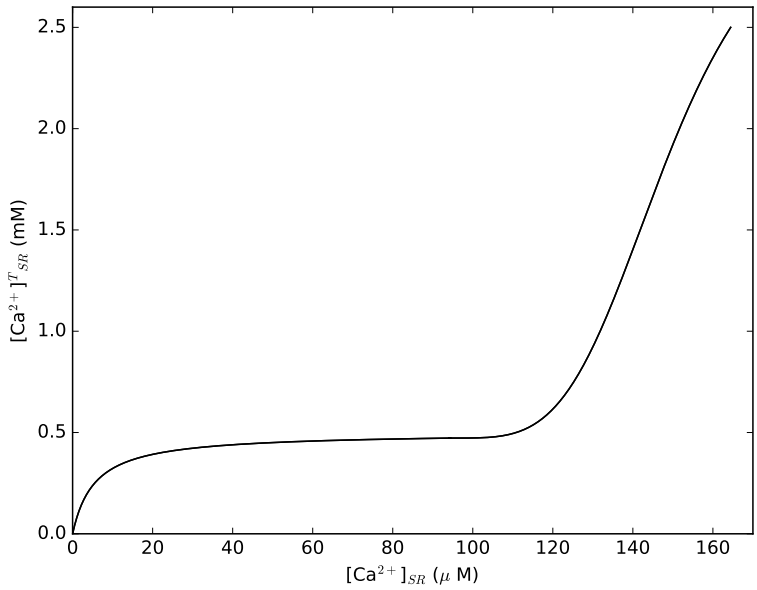

Figure 4.3: Total luminal calcium concentration vs free luminal calcium concentration. Graphical representation of equation (3.17) with parameters in the second column of table 3.1. Axes were exchanged to show the desired behavior.

The reason is that the function that relates $[Ca^{2+}]_{SR}$ with total luminal calcium we used, preserves in great extent the behavior that according to Pérez-Rosas [1] is the responsible for phase one. The positive concavity provided by the Hill function indicates an increase in the buffering capacity, and allows the system to use first the calcium that is bound to buffering proteins, rather than free calcium. Besides, given that the Hill function represents calcium in the pocket formed as a consequence of polymerization, to release it, calsequestrin must depolymerize as shown by Manno *et al.* in [16].

Application of 20 mM caffeine produces large variability in the amplitude, rate of rise and time to peak of $[Ca^{2+}]_i$ transients [10]. To reproduce this variability we varied the volume of the responding sarcoplasmic reticulum (parameter γ) from 1 % to 12 % as done by Pérez-Rosas *et al.* [10]. For each value of γ we calculated the amplitude of the calcium transient as the difference between the highest value of $[Ca^{2+}]_i$ and the basal $[Ca^{2+}]_i$; the time to peak as the time between the moment in which the pulse was applied and the highest value of $[Ca^{2+}]_i$; and the rate of rise as the quotient between them [1]. Figures 4.6**A)** and **B)** show rate of

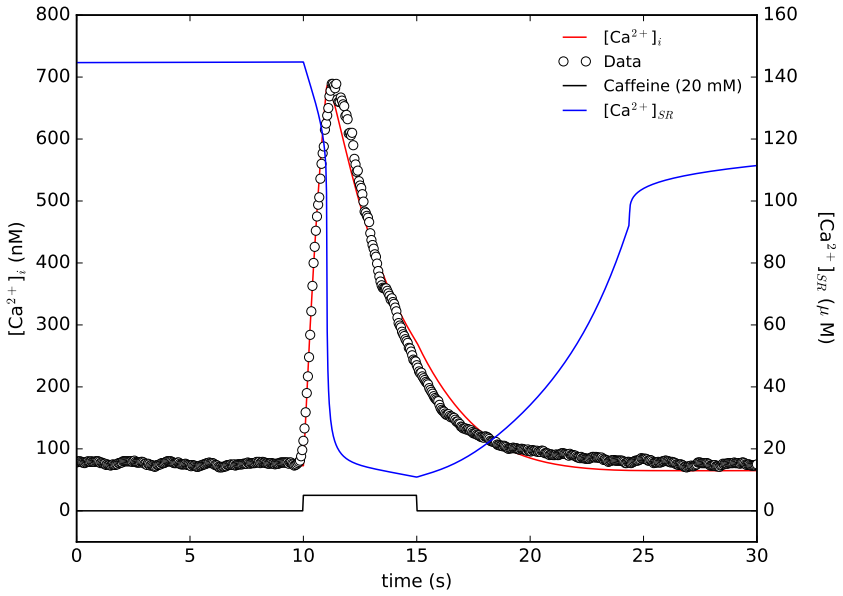

Figure 4.4: 20 mM caffeine pulse. Time course of calcium response to 20 mM of caffeine. Intracellular data [10] (circles) fitted by our model (red line) and luminal calcium reduction (blue line) in response to a 20 mM caffeine stimulus (black line).

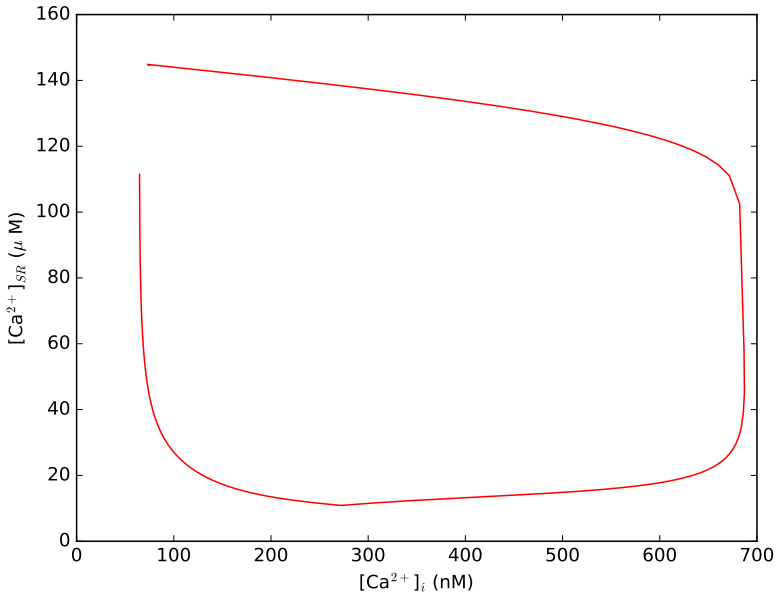

Figure 4.5: 20 mM caffeine phase diagram. Phase diagram of intracellular calcium versus luminal calcium during 20 mM caffeine pulse.

rise versus time to peak and rate of rise versus $[Ca^{2+}]_i$ amplitude response for 66 different cells (red circles) and the fitting with our model (black line). In both cases the behavior was

qualitatively reproduced by our model. However, we did not expect perfect fitting due to the fact that we are assuming that the only parameter that varies from cell to cell is γ, which is a very restrictive premise to begin with.

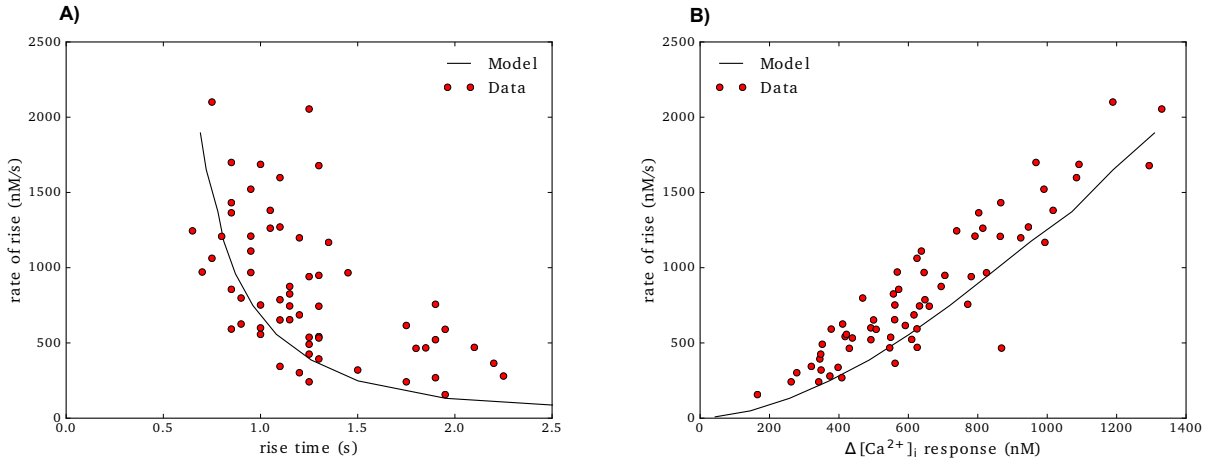

Figure 4.6: 20 mM caffeine pulse variability. A) Rate of rise versus time to peak. Experimental data [10] (red circles) for 66 different cells and fitting with our model (black line). **B)** Rate of rise versus $[Ca^{2+}]_i$ amplitude response.

4.3 Calsequestrin polymerization explains the refractory period associated with calcium recovery in the sarcoplasmic reticulum

Experiments performed by Dagnino-Acosta *et al.* [9] revealed that the sarcoplasmic reticulum presents a refractory period associated with calcium recovery. Our model reproduced those experiments for both $[Ca^{2+}]_i$ and $[Ca^{2+}]_{SR}$. Figure 4.7 shows experimental data [9] (blue line), data derived from the model (red line) and 20 mM caffeine pulse (black line).

Below we discuss why the total vs free calcium concentration function depicted in figure 4.3 allowed us to reproduce the experimental plots. First calcium released to the cytoplasm comes from calcium bound to calsequestrin dimers. After it runs out, calcium is released both from calsequestrin monomers and free luminal calcium, which produces the first peak in $[Ca^{2+}]_i$, and $[Ca^{2+}]_{SR}$ reduction. When refilling of the sarcoplasmic reticulum starts, both

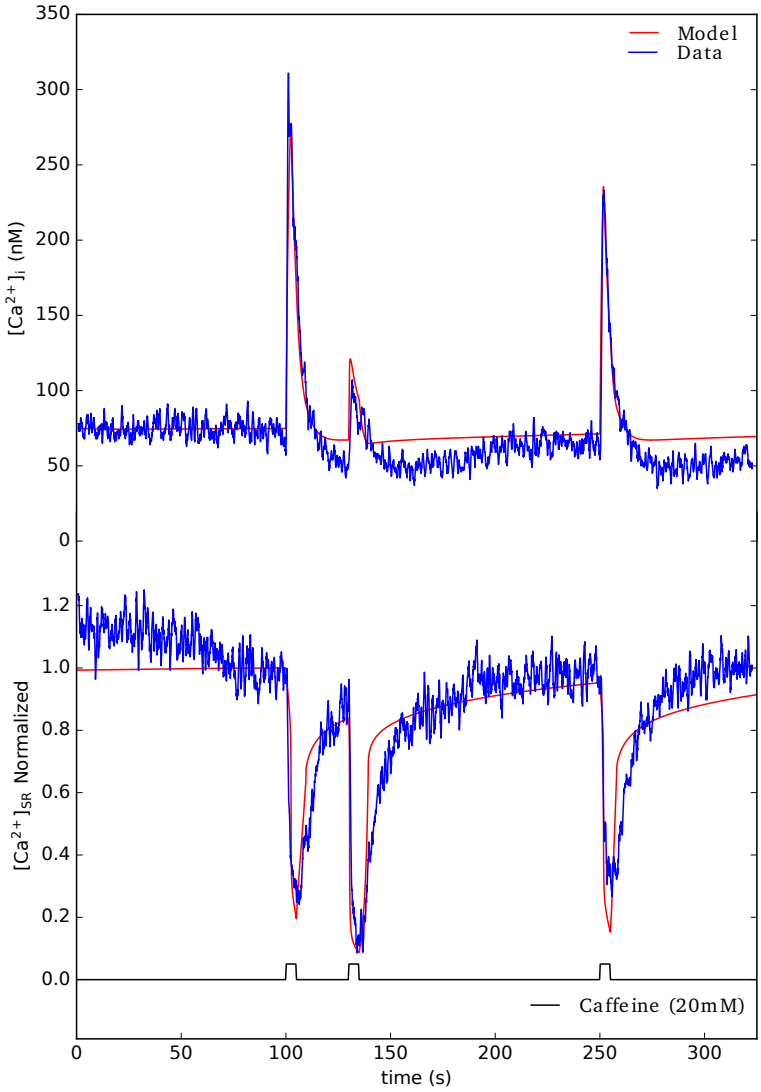

Figure 4.7: Caffeine-induced calcium release refractory response. Transients induced by caffeine show the refractory period associated with calcium recovery in the sarcoplasmic reticulum. Experimental data (blue), fitted by the model (red).

free luminal calcium and monomers start to fill simultaneously. Since monomers have a small number of binding sites they get saturated fast enough so that free luminal calcium is also quickly restored. Sufficient calcium is available to generate the next two peaks, but total luminal calcium is not completely restored since polymerization takes more time, which explains the refractory period. Pérez-Rosas *et al.* SK model [10] does not allow rapid free luminal calcium recovery. Even though calsequestrin has a finite number of binding sites, it is very large. As a result, saturation takes a very long time and so does free luminal calcium restoring. On the other hand, her KonD model allows rapid free luminal calcium recovery

but binding is very slow. Hence, not enough calcium is available to produce a satisfactory third peak as shown in figure 1.10.

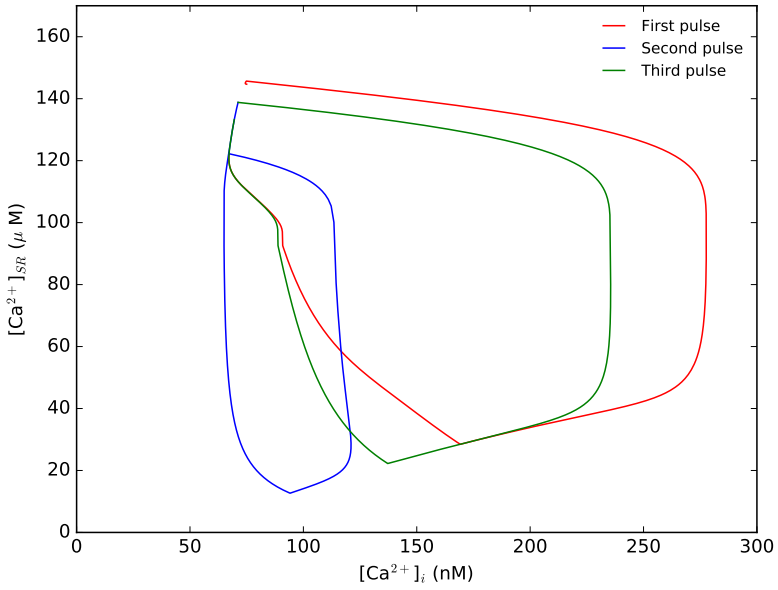

Figure 4.8: Phase diagram for a train of pulses. Phase diagram of data derived from the model for the three pulses in red, blue and green respectively.

Figure 4.8 shows the phase diagrams for the first (red line), second (green line) and third (blue line) pulse. First and third pulses show the four phases as seen experimentally [4]. In contrast, in the second pulse phase one has disappear almost completely and the behavior is somehow linear as shown by Guerrero-Hernández *et al.* [4]. Even though free luminal calcium has been restored after the first pulse, just few total luminal calcium has, which explains the short first phase followed by a large decrease in $[Ca^{2+}]_{SR}$.

4.4 Calsequestrin polymerization kinetics fits 2 mM caffeine-induced calcium release

Robustness of KonD model was evaluated by Pérez-Rosas [1] by using some of the same parameters used to reproduce the 20 mM caffeine-induced calcium response on a 2 mM re-

sponse. Our model reproduced the 2 mM by changing only caffeine concentration (table 3.2) as shown in figure 4.9. Calcium response (red line) took longer that for the previous experiment (section 4.2). Recovery of free luminal calcium was also slower (blue line). This can be explained considering $[Ca^{2+}]_i$ increased considerably more in this experiment, which caused total luminal calcium to decrease more too and hence $[Ca^{2+}]_{SR}$.

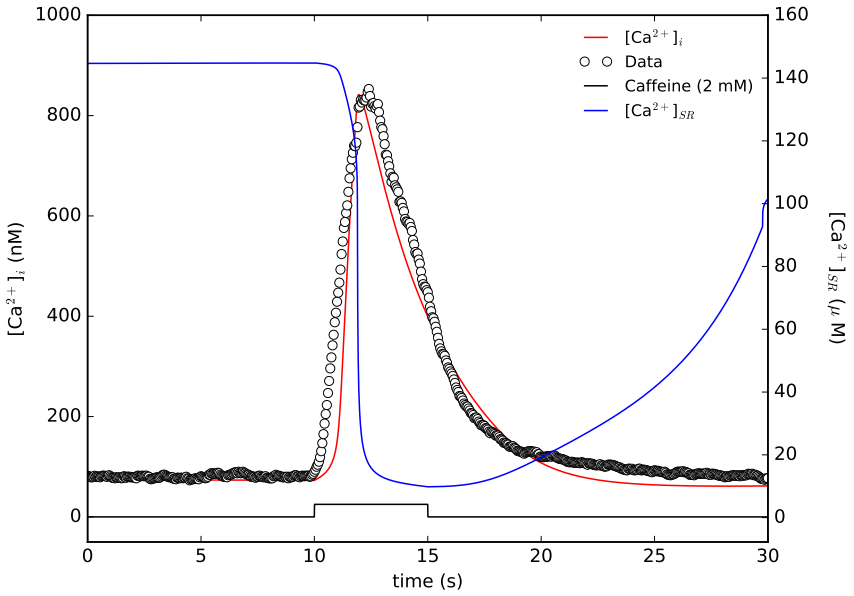

Figure 4.9: 2 mM caffeine pulse. Time course of calcium response to 2 mM of caffeine. Intracellular data [10] (circles) fitted by our model (red line) and luminal calcium reduction (blue line).

We also plotted the diagram phase for the 2 mM caffeine-induced response to make sure the four phases were still present as shown in figure 4.10.

We varied γ from 1 % to 10 % to reproduce variability. We calculated amplitude, rate of rise and time to peak in the same way as described in section 4.2. Figures 4.11**A)** and **B)** show experimental data (red circles) [10] for 49 different cells and data derived from the model (black line). Experimental data showed slower and smaller responses in contrast with those obtained during the 20 mM caffeine-induced experiments, that were reproduced with the model.

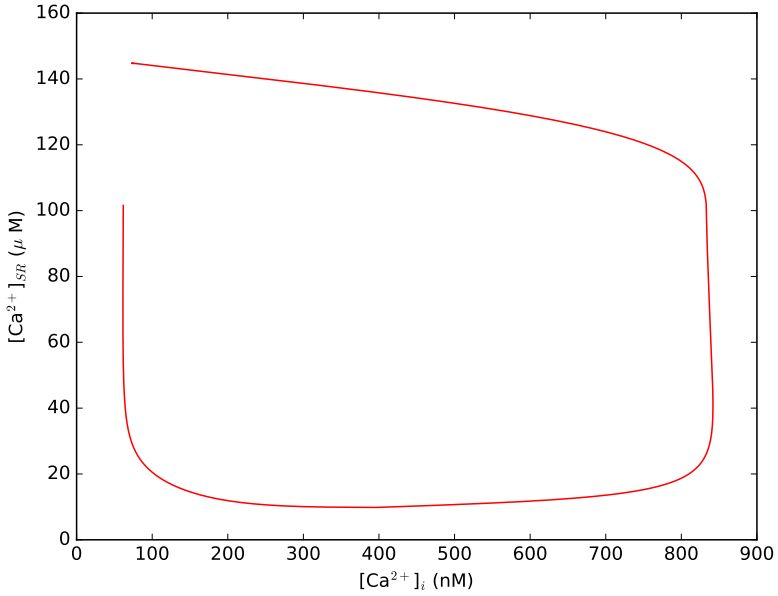

Figure 4.10: 2 mM caffeine phase diagram. Phase diagram of intracellular calcium versus luminal calcium during 2 mM caffeine pulse.

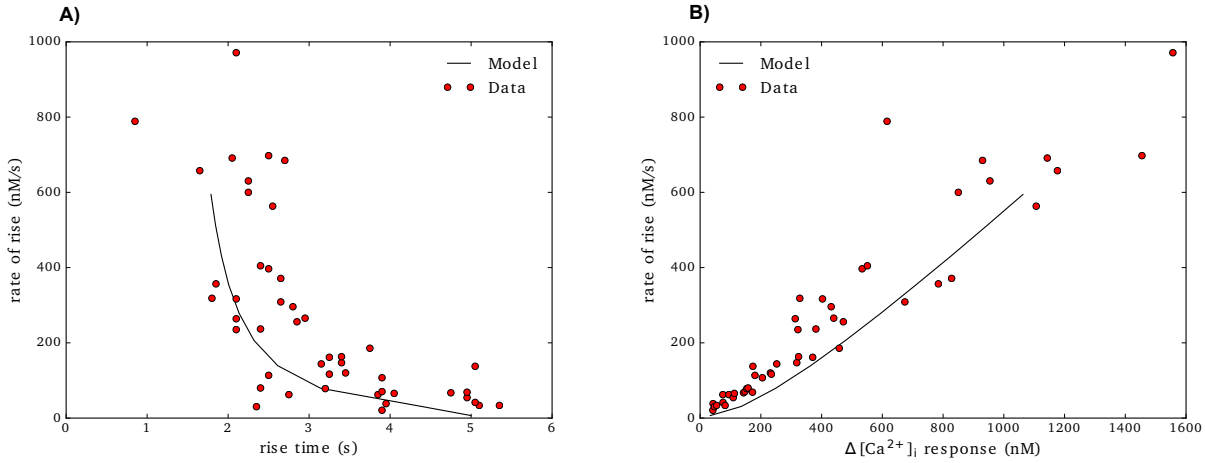

Figure 4.11: 2 mM caffeine pulse variability. A) Rate of rise versus time to peak. Experimental data [10] (red circles) for 49 different cells and fitting with our model (black line). **B)** Rate of rise versus $[Ca^{2+}]_i$ amplitude response.

4.5 Inhibition of SERCA pumps with thapsigargin affects calsequestrin depolymerization

In the experiment developed by Pérez-Rosas *et al.* [10] where SERCA pumps were inhibited using thapsigargin, evinced that the role of SERCA pumps does not limit to refilling the

sarcoplasmic reticulum, but they participate in calcium release too. Therefore we wondered what could be happening when SERCA pumps are blocked and considered different scenarios.

It is well known that there is calcium leakage from the sarcoplasmic reticulum into the cytoplasm [4]. One may think that the reticulum is depleting through the leakage, and as a consequence the caffeine-induced transient is smaller. Nonetheless, experiments performed in smooth muscle cells showed that applying thapsigargin did not modify basal concentrations in the cytoplasm nor in the reticulum, and a reduced transient was observed even when caffeine was applied up to 300 s later [17].

A second approach was to consider that the inhibition of SERCA pumps somehow affects RyRs. However, experiments showed that inducing calcium release through IP_3Rs after applying thapsigargin yielded the same response [17].

A third option would be that SERCA pumps blockage impacts on sequestering proteins in this case there are three options. It is not possible that only free luminal calcium is released from the sarcoplasmic reticulum because it is very little, and a transient of that amplitude will not be possible; if only calcium trapped inside the pockets and free luminal calcium were being released, the relationship between total luminal calcium and free luminal calcium will look like KonD (figure 1.5), which reproduces the four stages of calcium release (figure 1.8). Thus, we proposed that when SERCA pumps are blocked, calsequestrin dimers cannot break down. As a result, only calcium bound to monomers is released and calcium in the pockets formed during dimerization stays trapped as shown in figure 4.12.

Taking this consideration into account, in our expression that relates free luminal calcium with total luminal calcium (equation (3.17)) we eliminated the Hill equation and kept only the Michaleis-Menten one

$$[Ca^{2+}]_{SR} = K_m \frac{[Ca^{2+}]^T_{SR}}{M - [Ca^{2+}]^T_{SR}}. \tag{4.2}$$

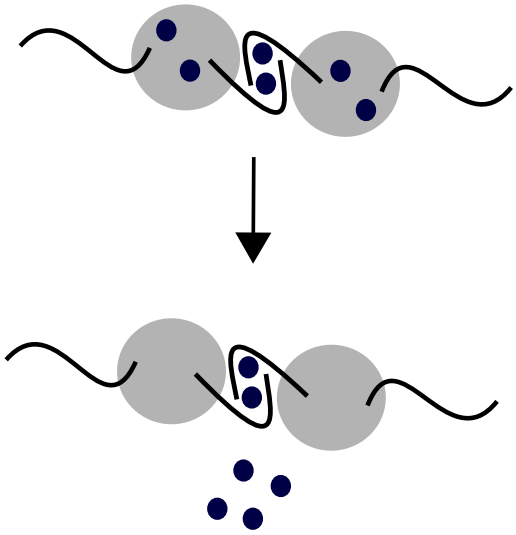

Figure 4.12: Calcium release when SERCA pumps are inhibited. When SERCA pumps are inhibited, calsequestrin cannot depolymerize, and calcium release is restricted to that bound to monomers.

Figure 4.13 shows the results.

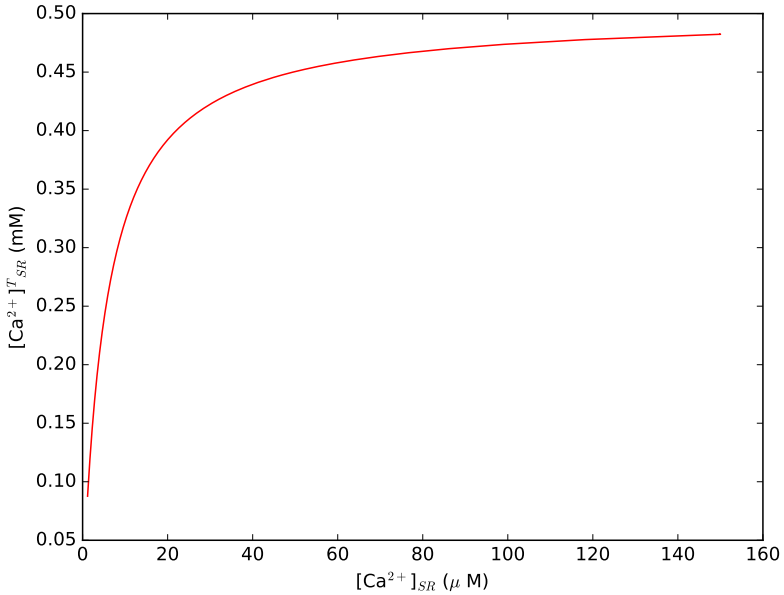

Figure 4.13: Total luminal calcium concentration vs free luminal calcium concentration with thapsigargin. Graphical representation of equation (4.2) with parameters in the third column of table 3.1. Axes were exchanged to show the desired behavior.

Figure 4.14 shows the time course of $[Ca^{2+}]_i$ response to 20 mM caffeine pulse after the cell was exposed to 10 µM of thapsigargin for five seconds [10]. Thapsigargin inhibits SERCA

pumps irreversibly by stabilizing them in the E2 state. Hence calcium in unable to bound and calcium concentration is not restored in the sarcoplasmic reticulum [1]. By shutting down flux J_3 (flux via SERCA pumps) we were able to reproduce the effect of SERCA pumps (blue line). Depletion of the sarcoplasmic reticulum was faster than in the 2 mM and 20 mM pulses. As we considered that only calcium bound to monomers was available as well as free luminal calcium, release of both of them starts almost simultaneously.

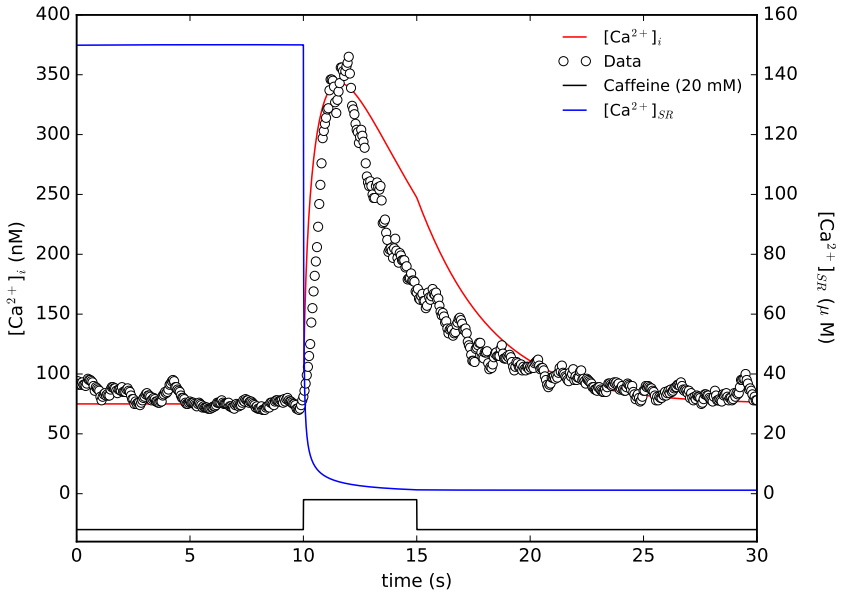

Figure 4.14: 10 µM thapsigargin and 20 mM caffeine pulse. Time course of calcium response to 20 mM of caffeine with previous exposure to 10 µM of thapsigargin. Intracellular data [10] (circles) fitted by our model (red line) and luminal calcium reduction (blue line).

Experiments [10] also showed that when SERCA pumps are inhibited, phase one of calcium release disappears. Figure 4.15 shows the phase diagram of *in silico* data from pulse in figure 4.14. Phase one has disappeared completely. Instead, there is simultaneous increase of $[Ca^{2+}]_i$ and decrease of $[Ca^{2+}]_{SR}$, directly related to the inverse Michaelis-Menten equation used to represent free luminal calcium. A second phase presents showing the recovery of basal concentration in the cytoplasm. Once again as expected, $[Ca^{2+}]_{SR}$ is not restored.

Variability was reproduced by varying γ from 1 % to 23 %. We calculated again for

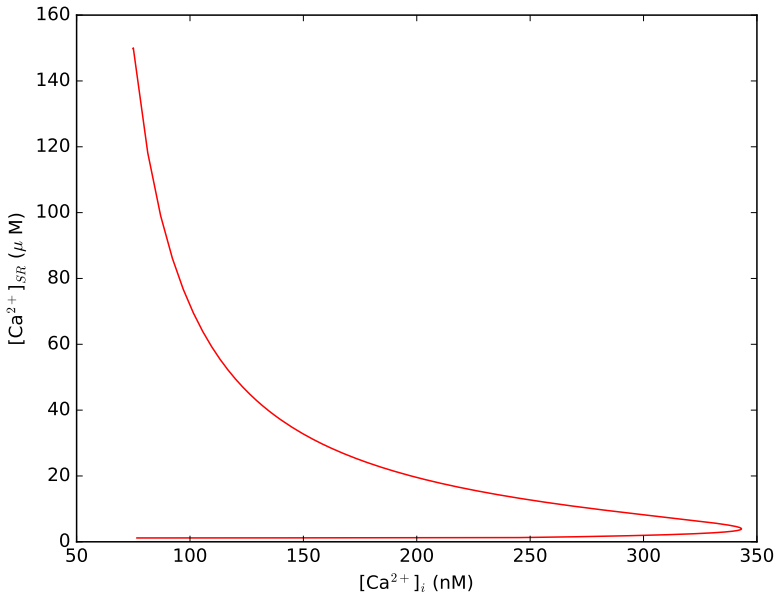

Figure 4.15: 10 µM thapsigargin and 20 mM caffeine phase diagram. Phase diagram of intracellular calcium versus luminal calcium during 20 mM caffeine pulse with previous exposure to 10 µM of thapsigargin.

each value of γ the amplitude, rate of rise and time to peak as described in section 4.2. Figures 4.16**A)** and **B)** show experimental data (red circles) [10] for 12 different cells and results obtained with the model (black line). Experiments with thapsigargin showed smaller rates than those without it, as well as smaller increases in $[Ca^{2+}]_i$ [1, 10] which our model reproduced. Once more we do not expect perfect fitting since the only parameter we varied was γ.

4.6 Calsequestrin inability to depolymerize when SERCA pumps are inhibited changes calcium release dynamics

As shown experimentally by Pérez-Rosas *et al.* in [10], inhibition of SERCA pumps changes the dynamics of calcium release in the sarcoplasmic reticulum. As mentioned in previous sections, our hypotheses (figure 4.17) allowed the model to reproduce the four phases of

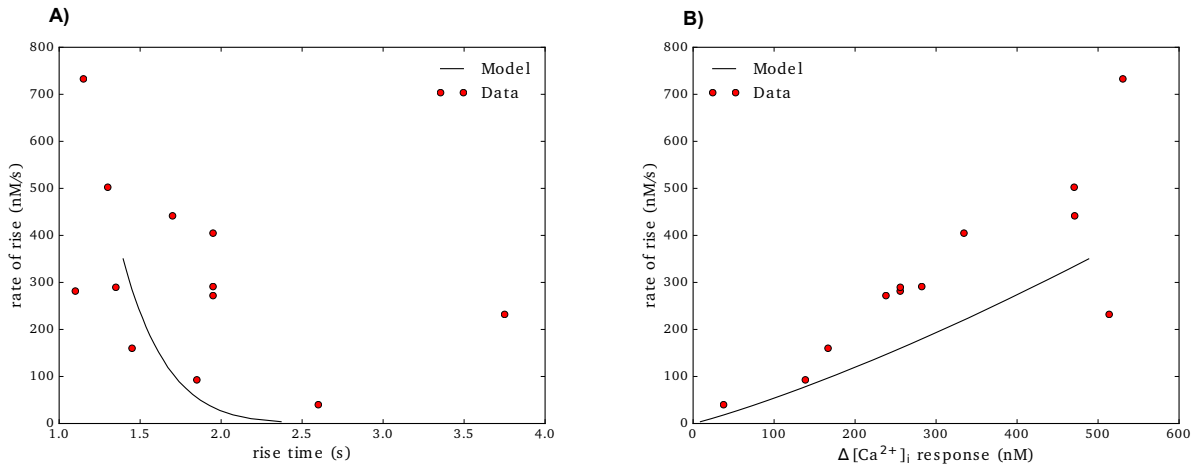

Figure 4.16: 10 µM thapsigargin and 20 mM pulse variability. A) Rate of rise versus time to peak. Experimental data [10] (red circles) for 12 different cells and fitting with our model (black line). **B)** Rate of rise versus $[Ca^{2+}]_i$ amplitude response.

calcium release without thapsigargin (figures 4.5 and 4.10), and the absence of them with thapsigargin (figure 4.15). However, experiments [10] showed that not only calcium release dynamics changed after applying thapsigargin, but calcium release overlapped with calcium recovery when thapsigargin was not applied. We observed, by plotting both phase diagrams obtained by us together, that even though they did not exactly overlap, the behavior was qualitatively the same (figure 4.18).

4.7 Calsequestrin polymerization kinetics provides an effective recovery dynamics for both total and free calcium basal concentrations

To obtain more information about the dynamics of the model discussed, one of our aims was to study its dynamic stability analytically by linearizing in a neighborhood of the equilibrium point. To tackle this issue, we proposed a comparison between our model (black line) and a hypothetic one where calsequestrin kinetics behaves according to a Michaelis-Menten function (red line) as shown in figure 4.19. To do so, in both cases we performed the following procedure. We first established the existence of a unique stationary state by analyzing the system of differential equations (described in section 3.1) analytically (see Appendix). Then

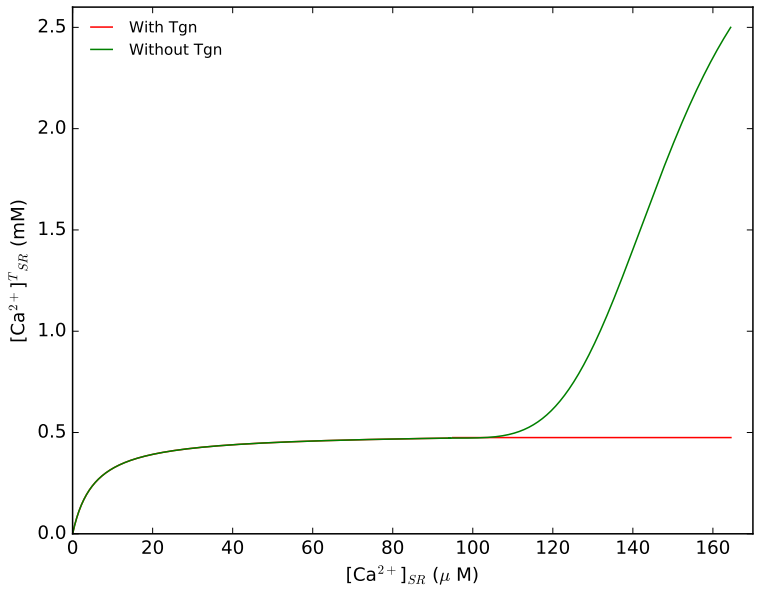

Figure 4.17: Total luminal calcium concentration vs free luminal calcium concentration with and without thapsigargin. Graphical representation of equations (3.17) and (4.2) with parameters in the second and third column of table 3.1 respectively. Axes were exchanged to show the desired behavior.

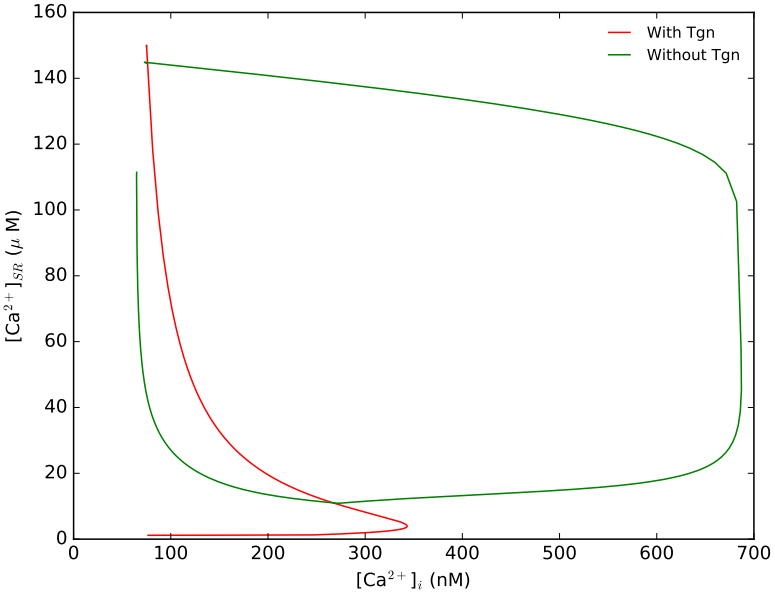

Figure 4.18: Phase diagrams for transients with and without thapsigargin. Phase diagrams of intracellular calcium versus luminal calcium during 20 mM caffeine pulse with and without previous exposure to 10 µM of thapsigargin.

we solved it (the model) for a sufficiently long time (t =1000 s) so that it reached the equilibrium, which gave us the value of the equilibrium point. For our model the equilibrium points were (7.49 µM, 1.65 mM) for total calcium and (7.49 nM, 1.45 µM), for free calcium. For the hypothetic model equilibrium points for total and free calcium were (7.50 µM, 1.65 mM) and (7.50 nM, 1.50 µM), respectively. Afterwards, we calculated de Jacobian of the system analytically and analyzed the stability of the stationary state. Finally, we plotted some of the phase plane trajectories varying the initial conditions 10 % around the equilibrium for both free and total calcium. We normalized the trajectories with respect to the equilibrium point for better comparison (figures 4.20, 4.21, 4.22 and 4.23).

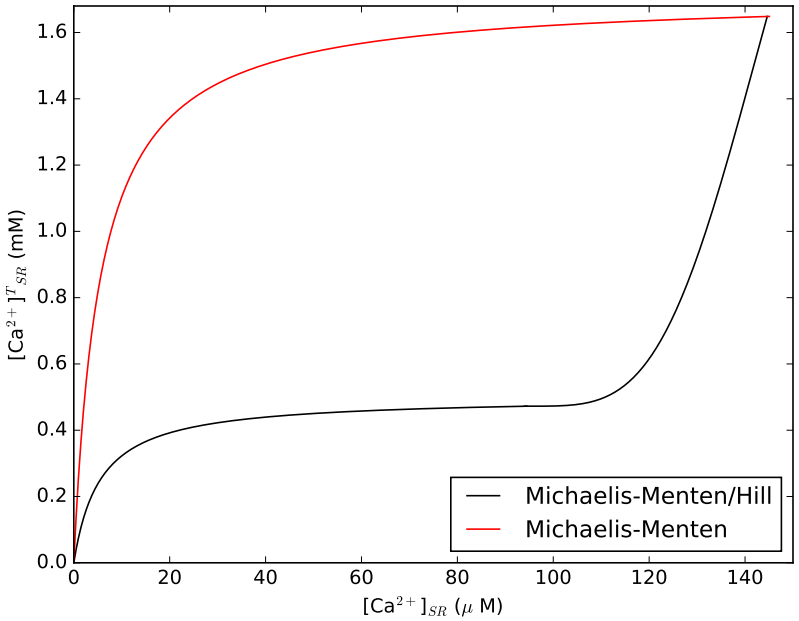

Figure 4.19: Total luminal calcium vs free luminal calcium for our Michaelis-Menten/Hill proposal and for a Michaelis-Menten approach. Relationship between total and free luminal calcium through calsequestrin polymerization kinetics (black line) and a Michaelis-Menten function (red line).

Recall that solving the model provides values for total cytoplasmic and luminal calcium. Analytically we determined that stationary states for both approaches were given by basal concentrations and in both cases they were stable. However, we found that for our model it was a node (even though it seems to be an improper node), whilst for the Michaelis-

Menten approach it was a spiral point which was later confirmed graphically (figures 4.20 and 4.21). This is very important because it tells us that our model has a more efficient total calcium recovery dynamics, compared to the Michaleis-Menten approach which needs several oscillations before reaching the equilibrium. We also observed that both cases present a manifold in which several trajectories converge on their way to the stability point.

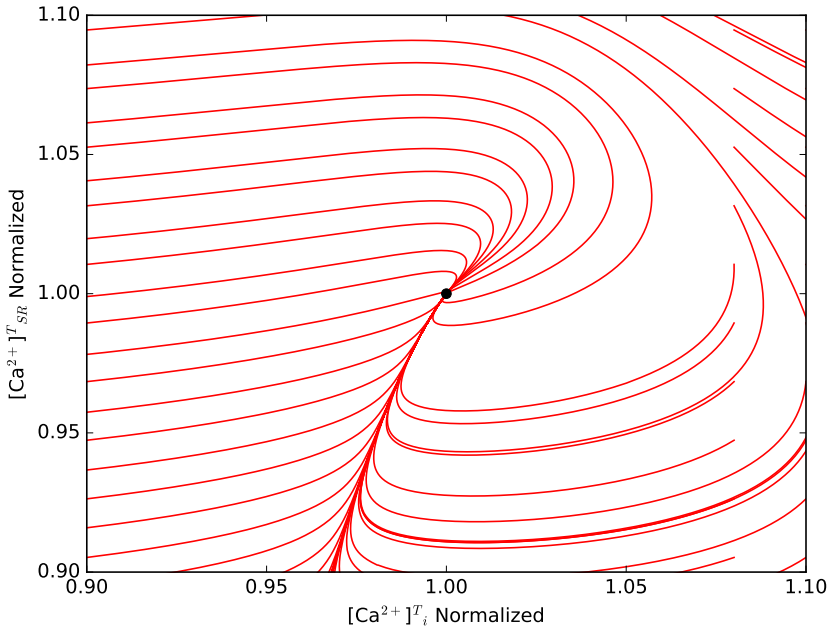

Figure 4.20: Total calcium phase plane trajectories for the Michaelis-Menten/Hill model. Equilibrium point (black) and normalized phase plane trajectories (red lines) of total calcium for our model showing an improper node. Variation for trajectories was 10 %.

Subsequently, we plotted the phase-plane trajectories for free cytoplasmic and luminal calcium and found that the described behavior was pretty much the same (figures 4.22 and 4.23). In spite of that, we could see that trajectories of our model for free calcium were somehow different from those for total calcium. For instance, the former are much closer along the vertical axis than the latter, and they are much more horizontal. This means that free luminal calcium basal levels are restored faster that total concentrations. In contrast, for the Michaelis-Menten approach things work the other way around. For both scenarios, free calcium phase plane trajectories present the manifold mentioned before.

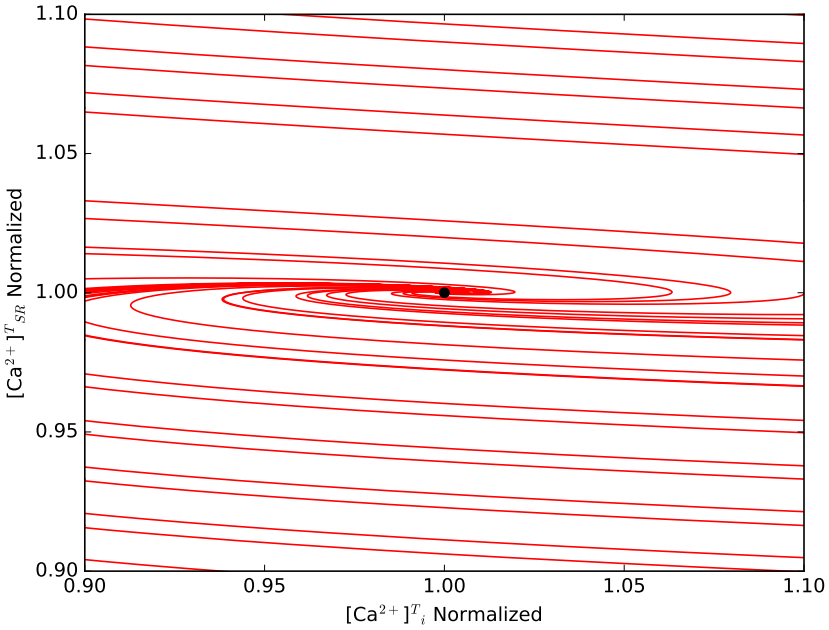

Figure 4.21: Total calcium phase plane trajectories for the Michaelis-Menten model. Equilibrium point (black) and normalized phase plane trajectories (red lines) of total calcium for the Michaelis-Menten approach showing a spiral point. Variation for trajectories was 10 %.

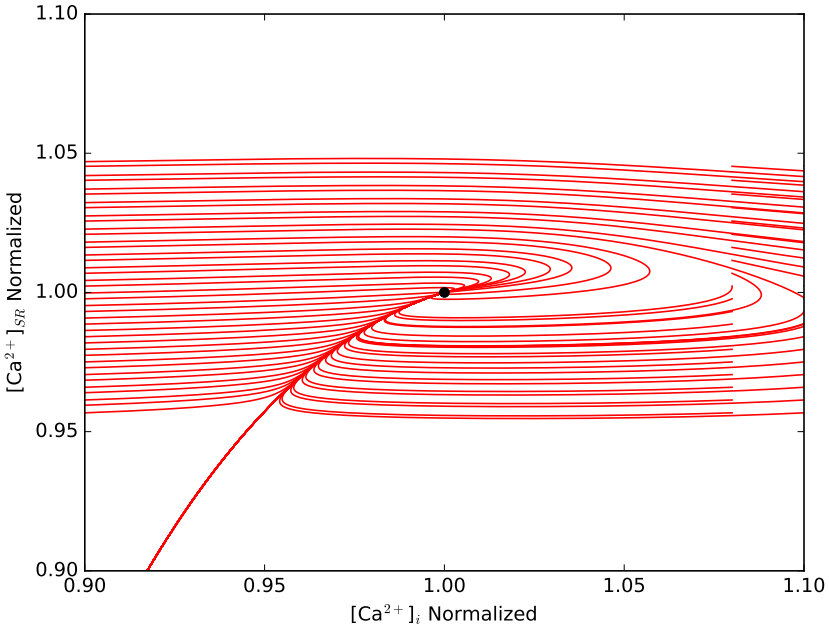

Figure 4.22: Free calcium phase plane trajectories for the Michaelis-Menten/Hill model. Equilibrium point (black) and normalized phase plane trajectories (red lines) of free calcium for our model showing an improper node. Variation for trajectories was 10 %.

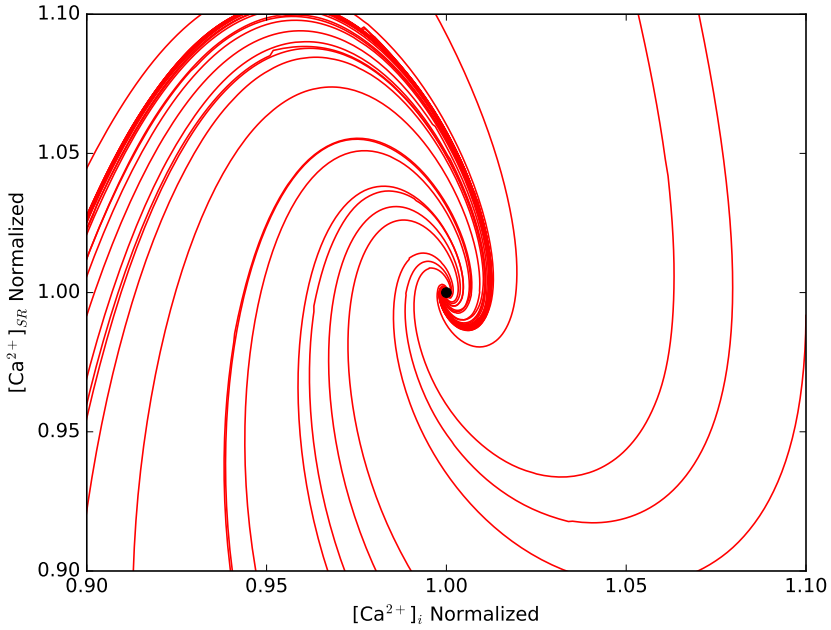

Figure 4.23: Free calcium phase plane trajectories for the Michaelis-Menten model. Equilibrium point (black) and normalized phase plane trajectories (red lines) of free calcium for the Michaelis-Menten approach showing a spiral point. Variation for trajectories was 10 %.

Chapter 5

Conclusions

Previous works on calcium dynamics propose that the high buffering capacity of the sarcoplasmic reticulum is possible because calsequestrin binds an infinitely large number of calcium ions. This work was aimed at stating an alternative explanation on how kinetics of sequestering proteins works taking into account their well known ability to form polymers. Several experiments suggest that calsequestrin polymerizes in response to increments in calcium concentration. Considering this, we developed an expression to relate total with free luminal calcium concentrations which included calsequestrin polymerization kinetics. We then incorporated this kinetics to an already developed mathematical model that describes calcium release dynamics from the sarcoplasmic reticulum of smooth muscle cells. Finally, we compared our findings to experimental data and analyzed the stability of the model. Our work led to the following conclusions:

- The kinetics of calcium-calsequestrin interaction and its polymerization can explain the dynamics of calcium release via ryanodine receptors in the sarcoplasmic reticulum of smooth muscle cells.
- Our results suggest that SERCA pumps inhibition prevents calsequestrin depolymerization, and does not allow release of calcium trapped in the pockets.
- Calsequestrin polymerization kinetics presents an efficient recovery of both total and free calcium basal concentrations.

Chapter 6

Perspectives

In this work we were interested in studying the kinetics inside the sarcoplasmic reticulum that explains its high buffering capacity. To do so, we tackled the issue through a mathematical approach by proposing a calcium-calsequestrin kinetics based on calsequestrin polymerization. Therefore, it would be really interesting to provide experimental evidence that supports the mechanisms of binding, unbinding, polymerization and depolymerization described in this work for both regular and post thapsigargin pulses.

In terms of simulations, the model could be tested on other cell types (not necessarily muscle cells) where calcium release is induced via different mechanisms. This in order to establish whether or not the kinetics described in this work is able to reproduce and describe experimental observations.

Bibliography

[1] N.C. Pérez Rosas. *Análisis de la dinámica del ion calcio durante su liberación por medio de los receptores de rianodina : un enfoque de modelación matemática*. Thesis, Centro de Investigación y de Estudios Avanzados del Instituto Politécnico Nacional, 2016.

[2] E. Carafoli. The calcium-signalling saga: tap water and protein crystals. *Nature Reviews Molecular Cell Biology*, 4:326 – 332, 2003.

[3] D.E. Clapham. Calcium Signaling. *Cell*, 131:1047 – 1058, 2007.

[4] A. Guerrero-Hernández, A. Dagnino-Acosta, and A. Verkhratsky. An intelligent sarco-endoplasmic reticulum Ca 2+ store: Release and leak channels have differential access to a concealed Ca 2+ pool. *Cell Calcium*, 48:143–149, 2010.

[5] G.E.N. Kass and S. Orrenius. Calcium Signaling and Cytotoxicity. *Environmental Health Perspectives*, 107(1):25 – 35, 1999.

[6] N.A. Beard, D.R. Laver, and A.F. Dulhunty. Calsequestrin and the calcium release channel of skeletal and cardiac muscle. *Progress in Biophysics and Molecular Biology*, 85(1):33–69, 2004.

[7] H.J. Park, Y.I. Park, E.J. Kim, B. Youn, K. Fields, A.K. Dunker, and C.H. Kang. Comparing skeletal and cardiac calsequestrin structures and their calcium binding: A proposed mechanism for coupled calcium binding and protein polymerization. *Journal of Biological Chemistry*, 279(17):18026–18033, 2004.

[8] A. Takahashi, P. Camacho, J.D. Lechleiter, and B. Herman. Measurement of Intracellular Calcium. *Physiological Reviews*, 79:1089 – 1125, 1999.

[9] A. Dagnino-Acosta and A. Guerrero-Hernández. Variable luminal sarcoplasmic reticulum Ca2+ buffer capacity in smooth muscle cells. *Cell Calcium*, 46(3):188–196, sep 2009.

[10] N.C. Pérez-Rosas, N.L. Gomez-Viquez, A. Dagnino-Acosta, M. Santillán, and A. Guerrero-Hernández. Kinetics on demand is a simple mathematical solution that fits recorded caffeine-induced luminal SR Ca2+ changes in smooth muscle cells. *PLoS ONE*, 10(9):1–22, 2015.

[11] M. Santillán. On the Use of the Hill Functions in Mathematical Models of Gene Regulatory Networks. *Mathematical Modelling of Natural Phenomena*, 3(2):85–97, oct 2008.

[12] J. Lytton, M. Westlin, S.E. Burk, G.E. Shull, and D.H. MacLennan. Functional comparisons between isoforms of the sarcoplasmic or endoplasmic reticulum family of calcium pumps. *Journal of Biological Chemistry*, 267(20):14483–14489, 1992.

[13] H. Mogami, J. Gardner, O.V. Gerasimenko, P. Camello, O.H. Petersen, and A.V. Tepikin. Calcium binding capacity of the cytosol and endoplasmic reticulum of mouse pancreatic acinar cells. *The Journal of physiology*, 518 (Pt 2:463–467, 1999.

[14] E. Neher. The Use: of Fura-for Estimating Fluxes Ca Buffers and Ca. *Neuropharmacology*, 34(11):1423–1442, 1995.

[15] Lan Wei, Amy D. Hanna, Nicole A. Beard, and Angela F. Dulhunty. Unique isoform-specific properties of calsequestrin in the heart and skeletal muscle. *Cell Calcium*, 45(5):474–484, 2009.

[16] C. Manno, L.C. Figueroa, D. Gillespie, R. Fitts, C. Kang, C. Franzini-Armstrong, and E. Rios. Calsequestrin depolymerizes when calcium is depleted in the sarcoplasmic reticulum of working muscle. *PNAS Plus*, pages E638 – E647, 2016.

[17] L. Gómez-Viquez, G. Guerrero-Serna, U. García, and A. Guerrero-Hernández. SERCA Pump Optimizes Ca 21 Release by a Mechanism Independent of Store Filling in Smooth Muscle Cells. *Biophysical Journal*, 85:370–380, 2003.

Appendix

Stability Analysis

Pérez-Rosas *et al.* [10] proposed model was given by the following ordinary differential equations system:

$$\frac{d[Ca^{2+}]_i^T}{dt} = -J_1 + J_2 - J_3, \tag{6.1}$$

$$\frac{d[Ca^{2+}]_{SR}^T}{dt} = \frac{J_3 - J_2}{\gamma}. \tag{6.2}$$

Recall that J_1 and J_3 are functions of $[Ca^{2+}]_i^T$, while J_2 is a function of both $[Ca^{2+}]_i^T$ and $[Ca^{2+}]_{SR}^T$. In order to determine de number of stationary states we set the system to zero. As a result, equation (6.2) becomes

$$J_2 - J_3 = 0. \tag{6.3}$$

By substituting equation (6.3) to equation (6.1) it follows that

$$\begin{aligned} J_1 &= 0, \\ a\left[[Ca^{2+}]_i^T - [\overline{Ca^{2+}}]_i\right] &= 0, \\ [Ca^{2+}]_i^T &= [\overline{Ca^{2+}}]_i. \end{aligned} \tag{6.4}$$

Replacing equation (6.4) in equation (6.3) we now have that J_3 is a constant function, while J_2 varies only according to $[Ca^{2+}]_{SR}^T$. Moreover, J_2 for both approaches (ours and the hypothetical Michaelis-Menten approach) is a monotonically increasing function. This means that

J_2 and J_3 can only intersect at most once. We plotted J_2 and J_3 as functions of $[Ca^{2+}]^T_{SR}$ to assure it (figures 6.1 and 6.2).

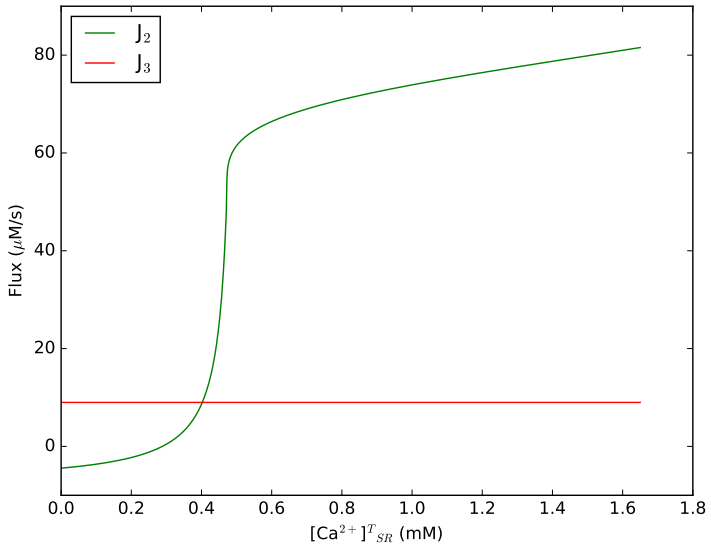

Figure 6.1: Unique stability for calsequestrin polymerization kinetics. Plot of J_2 (green line) and J_3 (red line) showing that there is unique stability for our calsequestrin polymerization kinetics approach.

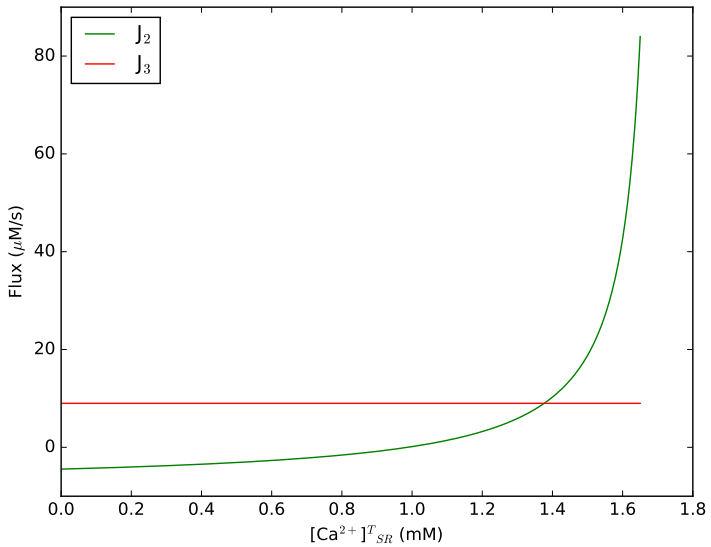

Figure 6.2: Unique stability for the hypothetical Michaelis-Menten kynetics. Plot of J_2 (green line) and J_3 (red line) showing that there is unique stability for the hypothetical Michaelis-Menten kinetics approach.